Thermodynamic modeling of boric acid and selected metal borate systems*

Peiming Wang‡, Jerzy J. Kosinski, Malgorzata M. Lencka,
Andrzej Anderko, and Ronald D. Springer

OLI Systems, Inc., 108 American Road, Morris Plains, NJ 07950, USA

Abstract: A comprehensive thermodynamic model, referred to as the mixed-solvent electrolyte (MSE) model, has been applied to calculate phase equilibria, speciation, and other thermodynamic properties of selected systems that are of interest for understanding the chemistry of salt lakes and natural waters. In particular, solubilities and chemical speciation have been analyzed for various boron-containing systems, which represent an important subset of solution chemistry for such applications. The model has been shown to reproduce the speciation, solubility, and vapor–liquid equilibrium (VLE) data in the boric acid + water system over wide ranges of temperature and concentration. Specifically, solubilities have been accurately represented in the full concentration range of the $B_2O_3 + H_2O$ system ($x_{B_2O_3} = 0\sim1$), which includes H_3BO_3. The accuracy of the model has also been demonstrated by calculating solubilities in various aqueous borate systems, i.e., $M_nO + B_2O_3 + H_2O$ (where M = Li, Na, Ca, Mg), and their mixtures with a chloride salt or an acid (i.e., LiCl, NaCl, HCl). The model predicts the effects of chemical speciation, temperature, and concentrations of various acid, base, and salt components on the formation of competing solid phases.

Keywords: borate; boric acid; phase equilibria; solubility; speciation; thermodynamic properties.

INTRODUCTION

The chemistry of boron-containing aqueous solutions is of interest for a number of practical applications. Aqueous boron species may be found in natural waters, including salt lakes, seawater, and hydrothermal fluids. Boric acid–borate buffers have been used as pH standards, in detergents, and in the coolants of pressurized water reactors. Boron chemistry also attracts considerable attention in energy applications because borohydrides of alkaline metals are potential hydrogen sources for fuel cells due to their high gravimetric hydrogen densities. Understanding the thermodynamics of boron-containing systems under the conditions relevant to these applications is important to facilitate an effective prediction of their chemical and phase behavior and to determine the optimum operating conditions for various processes where boron chemistry is involved.

Borate systems are known to be chemically complex due to the presence of a series of polyborate anions in addition to monomeric species as a result of chemical equilibria associated with hydrolysis and acid–base reactions. Boron-containing systems often exist together with various salts in multi-component electrolyte solutions at high concentrations under diverse conditions of temperature and

pressure. In addition, a number of stable or metastable solid phases may precipitate, depending on the solution concentration, ionic strength, pH, and temperature. Multiple experimental techniques have confirmed that the monomeric borate ion is the predominant anionic species in dilute aqueous solutions and in the absence of excess boric acid [1]. At the same time, polyborate species have been identified in a significant amount at higher total boron concentrations that may be found in crevice environments, spent fuel pools, and salt lakes [2–6]. Systems of this nature are challenging for computational models because of complicated chemical speciation, solution nonideality, and complex phase behavior (e.g., the formation of multiple hydrated salts or double salts and the presence of eutectic points). In view of the practical importance of mixed electrolyte systems, various electrolyte models have been reported in the literature and applied to the calculation of phase equilibria and other thermodynamic properties [7,8]. In a realistic electrolyte model, a comprehensive and self-consistent treatment of speciation is of utmost importance because phase equilibria and other thermodynamic properties are often inextricably linked to speciation equilibria due to ion pairing, hydrolysis, acid–base reactions, and other phenomena.

In this study, we apply a previously developed speciation-based thermodynamic model [7,9] to the boron-containing systems that are of practical interest. This model, referred to as MSE (mixed-solvent electrolyte) model, was previously shown to reproduce simultaneously vapor–liquid, solid–liquid, and liquid–liquid equilibria, speciation, caloric, and volumetric properties of electrolytes in water, organic, or mixed solvents [10,11]. The MSE model has been developed to be equally valid for classical aqueous systems, those with more than one distinct solvent and those in which a given component may continuously vary from being a solute to being a solvent (e.g., in acid–water mixtures). This is an important advantage over other available activity coefficient models, such as the well-known molality-based model of Pitzer [12], which represents solution properties for concentrations up to only 6 molal for most electrolyte solutions. The MSE model is capable of representing phase equilibria in multi-component inorganic systems containing multiple salts, acids, and bases [10,13–19] and in ionic liquid systems [20].

The systems analyzed in this work include the H_3BO_3/HBO_2/B_2O_3 + water mixtures in the full composition range that covers $x_{H_3BO_3}$ from 0 to 1 and, more generally, $x_{B_2O_3}$ from 0 to 1. Further, a model is established for the borate salt systems that are commonly encountered in natural waters, i.e., those involving the Li, Na, Ca, and Mg cations. Rather than focusing on particular processes, the current work is to provide a comprehensive treatment on the basis of the available experimental thermodynamic data for such systems. The model is used to represent the properties of binary and multicomponent systems, especially solubilities, under varying conditions and in the presence of other salts and acids. It is applied to reproduce the effects of system variables such as temperature, salt, acid, or base concentration on the solubility behavior of various solids. In particular, solubilities of boric acid (H_3BO_3), metaboric acid (HBO_2), and boron trioxide (B_2O_3) in water and acid solutions are examined together with vapor–liquid equilibrium (VLE) data (e.g., boiling points and volatilities). These results provide a thermodynamic foundation to explain natural variations in salt deposits or brine evaporation, to predict mineral equilibria in natural waters, and to evaluate how the properties of natural waters and industrial working fluids may affect various processes such as hydrothermal deposit formation and immobilization of waste effluents.

THERMODYNAMIC FRAMEWORK

Details of the thermodynamic model have been described elsewhere [9,11], and, therefore, only a brief summary is given here. The thermodynamic framework combines an excess Gibbs energy model for MSE systems with a detailed treatment of chemical equilibria. The excess Gibbs energy is expressed as

$$\frac{G^{ex}}{RT} = \frac{G^{ex}_{LR}}{RT} + \frac{G^{ex}_{II}}{RT} + \frac{G^{ex}_{SR}}{RT} \tag{1}$$

where G_{LR}^{ex} represents the contribution of long-range electrostatic interactions, G_{II}^{ex} accounts for specific ionic (ion–ion and ion–molecule) interactions and G_{SR}^{ex} is a short-range contribution resulting from intermolecular interactions. The long-range interaction contribution is calculated from the Pitzer–Debye–Hückel formula [12] expressed in terms of mole fractions and symmetrically normalized. The short-range interaction contribution is calculated from the UNIQUAC equation [21]. The specific ion–interaction contribution is calculated from an ionic strength-dependent, symmetrical second virial coefficient-type expression [9]

$$\frac{G_{II}^{ex}}{RT} = -\left(\sum_i n_i\right) \sum_i \sum_j x_i x_j B_{ij}(I_x) \tag{2}$$

where $B_{ij}(I_x) = B_{ji}(I_x)$, $B_{ii} = B_{jj} = 0$ and the ionic strength dependence of B_{ij} is given by

$$B_{ij}(I_x) = b_{ij} + c_{ij}\exp\left(-\sqrt{I_x + a_1}\right) \tag{3}$$

where b_{ij} and c_{ij} are adjustable parameters and a_1 is set equal to 0.01. The parameters b_{ij} and c_{ij} are calculated as functions of temperature as

$$b_{ij} = b_{0,ij} + b_{1,ij}T + b_{2,ij}/T + b_{3,ij}T^2 + b_{5,ij}\exp(b_{6,ij}T) + b_{7,ij}T\ln T + b_{8,ij}/\exp(b_{9,ij}T) \tag{4}$$

$$c_{ij} = c_{0,ij} + c_{1,ij}T + c_{2,ij}/T + c_{3,ij}T^2 + c_{5,ij}\exp(c_{6,ij}T) + c_{7,ij}T\ln T + c_{8,ij}/\exp(c_{9,ij}T) \tag{5}$$

For most electrolyte systems, the first three terms (i.e., $b_{0,ij}$, $b_{1,ij}$, $b_{2,ij}$ and $c_{0,ij}$, $c_{1,ij}$, $c_{2,ij}$) are sufficient for representing the variations of properties with temperature over a temperature range up to 300 °C. Additional temperature-dependent parameters are necessary only for a limited number of systems for which data analysis needs to be performed over an extended range of temperatures. In cases where data analysis needs to be extended to very high pressures, a pressure-dependent interaction parameter may also be introduced. In such cases, a linear function of pressure is sufficient. Then, eq. 4 can be extended to include a pressure-dependent term:

$$b_{ij} = b_{0,ij} + b_{1,ij}T + b_{2,ij}/T + b_{3,ij}T^2 + b_{5,ij}\exp(b_{6,ij}T) + b_{7,ij}T\ln T + b_{8,ij}/\exp(b_{9,ij}T) + \tag{4a}$$
$$(b_{2p,ij}/T)P$$

where the last term introduces a linear function of pressure that is also dependent on temperature.

For electrolyte systems encountered in natural waters such as salt lakes, seawater, hydrothermal fluids, and in other systems where the ionic strength and concentrations of boric acid and borate ions are significant, the specific ion–interaction contribution is the most important one to reproduce the properties of the solutions. When a chemical process occurs in a mixed solvent or in solutions where undissociated inorganic acids or bases are present in significant amounts, the short-range contribution is introduced to account for molecular interactions between the undissociated acid (or base) and the solvent molecules or between solvent components. It should be noted that the G_{II}^{ex} term can also be applied to non-ionic mixtures or weakly ionized systems, and has been found to improve the simultaneous fit to multiple properties in non-electrolyte systems when B_{ij} is introduced between two neutral molecules [11].

While the excess Gibbs energy model is used to calculate nonideality effects on solution properties, the chemical equilibrium is governed by the chemical potentials of all species that participate in various reactions, such as precipitation, hydrolysis, and ion-pairing. The chemical potential of each ionic or neutral species i is determined by its standard-state chemical potential, $\mu_i^0(T,P)$ and its activity coefficient, $\gamma_i(T,P,x)$, i.e.,

$$\mu_i(T,P,x) = \mu_i^0(T,P) + RT\ln x_i\gamma_i(T,P,x) \tag{6}$$

The standard-state chemical potentials of aqueous species, $\mu_i^0(T,P)$, are calculated as functions of temperature and pressure using the Helgeson–Kirkham–Flowers (HKF) equation of state [22–24]. The

parameters of the HKF model are available for various aqueous species [25,26]. The standard-state properties calculated from the HKF model are based on the infinite-dilution reference state and on the molality concentration scale. To make the equilibrium calculations consistent when the standard-state properties are combined with the mole fraction-based and symmetrically normalized activity coefficients, two conversions are performed [9]:

(1)   The activity coefficients calculated from eq. 1 are converted to those based on the unsymmetrical reference state, i.e., at infinite dilution in water:

$$\ln \gamma_i^{x,*} = \ln \gamma_i^x - \lim_{\substack{x_i \to 0 \\ x_w \to 1}} \ln \gamma_i^x \tag{7}$$

where $\lim_{\substack{x_i \to 0 \\ x_w \to 0}} \ln \gamma_i^x$ is the value of the symmetrically-normalized activity coefficient at infinite dilu-

tion in water, which is calculated by substituting $x_i = 0$ and $x_w = 1$ into the activity coefficient equations and

(2)   The molality-based standard-state chemical potentials are converted to corresponding mole fraction-based quantities:

$$\mu_i^{L,0,x}(T,P) = \mu_i^{L,0,m}(T,P) + RT \ln \frac{1000}{M_{\mathrm{H_2O}}} \tag{8}$$

where $M_{\mathrm{H_2O}}$ is the molecular weight of water. The values of $\ln \gamma_i^{x,*}$ and $\mu_i^{L,0,x}$ from eqs. 7 and 8 are then used in eq. 6 to determine the chemical potential of each species for chemical equilibrium calculations. Thus, the calculations require the availability of parameters for both the standard-state properties and activity coefficients.

DETERMINATION OF MODEL PARAMETERS

The combined thermodynamic framework has been applied to model the phase behavior of binary and mixed B_2O_3 + OH + M + H_2O systems (where M = Na, Li, Ca, Mg) with or without additional chloride components (i.e., NaCl, LiCl, or HCl). Tables 1–4 summarize the primary literature sources that were used for developing the model, together with their temperature, pressure, and salt content ranges. The parameters of the models have been determined using thermodynamic data of various types, including: (1) VLE; (2) water activity (a_w) or osmotic coefficients (ϕ); (3) solubility of solids in water or aqueous acids, bases, and other salts; (4) speciation data, such as pH and equilibrium constants; (5) volumetric data; and (6) caloric data such as heat capacities. The use of multiple data types is important to ensure the accuracy of model parameters. For example, caloric data are useful to determine the temperature dependence of model parameters. This makes it possible to make reliable predictions of solubilities well beyond the temperature range of experimental data.

For binary and multicomponent Na + Li + Mg + Ca + Cl + H + H_2O systems (i.e., without boron species), the MSE parameters were determined in previous studies [9,14]. These parameters ensure that the model reproduces the phase equilibria and caloric properties of binary, ternary, and multicomponent mixtures from the freezing point up to 300 °C and from infinite dilution to solid saturation or fused salt limit. Parameters that determine the thermodynamic properties of individual species in these systems (i.e., the standard partial molar Gibbs energy of formation, entropy, and parameters of the HKF equation of state) as well as the binary interaction parameters (eqs. 4 and 5) between the species have been reported in a previous paper [14]. These species include the individual ions (i.e., Na^+, Li^+, Mg^{2+}, Ca^{2+}, and Cl^-) and the ion pairs (i.e., $MgCl_{2(aq)}$, $CaCl_{2(aq)}$, $LiCl_{(aq)}$, $HCl_{(aq)}$) that were taken into account in the previous studies [9,14].

Table 1 Literature data sources for modeling the $H_3BO_3/HBO_2/B_2O_3 + H_2O$ system. The symbols m_s and x_s denote the saturation molality and mole fraction, respectively.

System	Reference	Type of data	T, K	P, atm	Concentration range
$H_3BO_3 + H_2O$	Kukuljan et al. [37]	VLE	452–645	P_{sat}	$m_{H_3BO_3} = 0.02–0.11$
or	von Stackelberg et al. [38]	VLE, solubility	373–376	1	$m_{H_3BO_3} = 1.1–6.1$ and
$B_2O_3 + H_2O$			441–474	P_{sat}	m_s
	Dukelski [29]	solubility	303	1	m_s
	Blasdale and Slansky [27]	solubility	273–376	1	m_s
	Chanson and Millero [28]	solubility	298	1	m_s
	Menzel [30]	solubility	272–298	1	m_s
	Nies and Hulbert [34]	solubility	272–376	1	m_s
	Platford [35]	solubility, ϕ	298	P_{sat}	$m_{H_3BO_3} = 0.0033 - m_s$
	Benrath [31]	solubility	272–454	P_{sat}	x_s up to 1.0
	Kracek et al. [36]	solubility	338–723	P_{sat}	x_s up to 1.0
	Nasini and Ageno [33]	solubility, VLE	272–393	P_{sat}	$m_{H_3BO_3} = 0.34 - m_s$
	McCulloch [32]	solubility	385–738	P_{sat}	x_s up to $x_{B_2O_3} = 0.98$ (covers $x_{H_3BO_3}$ to 1.0)
	Ganopolsky et al. [43]	V	375–523	6–55	$m_{H_3BO_3} = 0.06–0.5$
	Abdulagatov and Azizov [41]	V	296–573	8–474	$m_{H_3BO_3} = 0.06–0.5$
	Corti et al. [1]	V	298, 318	1	$m_{H_3BO_3} < 0.05$
	Hnedkovsky et al. [44]	V, C_p	298–705	1–345	$m_{H_3BO_3} = 0.2–0.75$
	Mesmer et al. [4]	equilibrium constants	323–563	P_{sat}	$I(KCl) = 0\sim1$ m
	Macdonald et al. [39,40]	pH	298–548	P_{sat}	$m_{H_3BO_3} = 0.001–0.1$

Table 2 Literature data sources for modeling the $H_3BO_3 + M(OH)_n + M$-borate $+ H_2O$ systems (M = Li, Na). The symbol m_s denotes the saturation molality.

System	Reference	Type of data	T, K	P, atm	Concentration range
$H_3BO_3 + LiOH + H_2O$	Rollet and Bouaziz [63]	solubility	303	1	m_s
	Bouaziz [64]	solubility	303–373	1	m_s
	Dukelski [29]	solubility	303	1	m_s
	Reburn and Gale [61]	solubility	273–374	1	m_s
$Li_2B_4O_7 + H_2O$	Reburn and Gale [61]	solubility	273–373	1	m_s
	Zhang et al. [65]	ϕ, solubility	298	P_{sat}	$m_{Li_2B_4O_7} = 0.027\sim m_s$
	Sang et al. [66]	solubility	288	1	m_s
	Menzel [67]	freezing point	271–273	1	$m_{Li_2B_4O_7} = 0.03\sim0.23$
$LiBO_2 + H_2O$	Reburn and Gale [61]	solubility	273–374	1	m_s
	Menzel [67,68]	solubility, FP	272–298	1	m_s

Table 2 (Continued).

System	Reference	Type of data	T, K	P, atm	Concentration range
$LiB_5O_8 + H_2O$	Byers et al. [69]	solubility	573–633	204	m_s
	Reburn and Gale [61]	solubility	318–353	1	m_s
	Menzel [67]	freezing point	271–273	1	$m_{LiB_5O_8} = 0.045{\sim}0.33$
$B_2O_3 + Na_2O + H_2O$	Linke and Seidell [70]	solubility	273–363	1	m_s
	Nies and Hulbert [34]	solubility	273–393	P_{sat}	m_s
	Rosenheim and Leyser [71]	solubility	273	1	m_s
	Dukelski [29]	solubility	303	1	m_s
	Rothbaum et al. [72]	pH	293–313	1	$m_{Na_2O} = 0.90{\sim}3.8$ $m_{B_2O_3} = 0.82{\sim}13.4$
	Weres [73]	a_w	550, 590	P_{sat}	m_s
$Na_2B_4O_7 + H_2O$	Urusova and Valyashko [74]	solubility, VLE	472–698	P_{sat}	m_s
	Kemp [75]	pH	293	1	$m_{Na_2B_4O_7} = 0.005{\sim}0.1$
	Apelbalt and Manzurola [76]	solubility, VLE	272–364	P_{sat}	m_s
	Platford [35]	ϕ	298	P_{sat}	$m_{Na_2B_4O_7} = 0.01{\sim}1.2$
	Menzel [67,77]	freezing point	272–273	1	$m_{Na_2B_4O_7} = 0.01{\sim}0.08$
	Teeple [78]	solubility	293–308	1	m_s
$NaBO_2 + H_2O$	Menzel [67,77]	freezing point	272–273	1	$m_{NaBO_2} = 0.04{\sim}0.33$
	Kemp [75]	pH	293	1	$m_{NaBO_2} = 0.02{\sim}2.0$
	Mashovets et al. [79]	VLE	423–573	P_{sat}	$m_{NaBO_2} = 0{\sim}3.8$
	Platford [35]	ϕ	298	P_{sat}	$m_{NaBO_2} = 0.1{\sim}4.0$
	Teeple [78]	solubility	293–308	1	m_s
$NaH_4B_5O_{10} + H_2O$	Kemp [75]	pH	293	1	$m_{NaH_4B_5O_{10}} = 0.04{\sim}0.5$
$Na_2B_4O_7 + NaBO_2 + H_2O$ $Na_2B_4O_7 + H_3BO_3 + H_2O$	Teeple [78]	solubility	293–308	1	m_s

Table 3 Literature data sources for modeling the $B_2O_3 + MO + H_2O$ systems (M = Ca, Mg). The symbol m_s denotes the saturation molality.

System	Reference	Type of data	T, K	P, atm	Concentration range
$CaO–B_2O_3–H_2O$	Kurnakova [80]	solubility	298	1	m_s
	Rza-Zade & Ganf [81,82]	solubility	298, 318	1	m_s
	Nikolaev and Chelishcheva [83]	solubility	298	1	m_s
	Mandelbaum [84]	solubility	303–363	1	m_s
	Nikolskii and Plyschevskii [85]	solubility	298–368	1	m_s
	Sborgi [86]	solubility	303	1	m_s
$MgO–B_2O_3–H_2O$	Kurnakova [80]	solubility	298	1	m_s
	Rza-Zade et al. [87]	solubility	298	1	m_s
	Rza-Zade et al. [88]	solubility	318, 343	1	m_s
	Nikolaev and Chelishcheva [83]	solubility	298	1	m_s
	D'Ans and Behrendt [89]	solubility	298–356	1	m_s

Table 4 Experimental data used for modeling the $B–M–Cl–H–OH–H_2O$ systems (M = Na, Li, H).

System	Reference	Type of data	T, K	P, atm	Salt concentration
$H_3BO_3–NaCl–H_2O$	Linderstrom-Lang [90]	solubility	285–297	1	$m_{NaCl} = 0{\sim}3.55$
	Di Giacomo et al. [91]	solubility	303–373	1	$m_{NaCl} = 0.68{\sim}6.9$
	Herz [92]	solubility	298	1	$m_{NaCl} = 0{\sim}3.3$
	Serduk [93]	solubility	298	1	$m_{NaCl} = 0{\sim}6.2$
	Teeple [78]	solubility	308, 348	1	$m_{NaCl} = 6.3{\sim}6.6$
$H_3BO_3–LiCl–H_2O$	Gode and Klavina [94]	solubility	298	1	$m_{LiCl} = 0{\sim}20.9$
	Herz [92]	solubility	298	1	$m_{LiCl} = 0{\sim}4.1$
	Linke and Seidell [70]	solubility	285–298	1	$m_{LiC} = 0{\sim}6.1$
$H_3BO_3–HCl–H_2O$	Kendall [95]	solubility	298	1	$m_{HCl} = 0{\sim}15.6$
	Herz [92,96]	solubility	298	1	$m_{HCl} = 0{\sim}12.1$
	Linke and Seidell [70]	solubility	291	1	$m_{HCl} = 0{\sim}1.58$
$Na_2B_4O_7–NaBO_2–H_3BO_3–NaCl–H_2O$	Teeple [78]	solubility	293–308	1	$m_{NaCl} = 2.2{\sim}6.2$
$NaBO_2{\cdot}5B_2O_3–NaCl–H_2O$	Peng [97]	soubility	273–373	1	$m_{NaCl} = 0.18{\sim}6.36$
$NaBO_2–NaCl–H_2O$	Skortsov et al. [62]	solubility	293	1	$m_{NaCl} = 0{\sim}6.13$
$Na_2O–H_3BO_3–NaCl–H_2O$	Kuka and Gode [98]	solubility, pH	298	1	$m_{NaCl} = 3.62{\sim}4.38$

In the present study, we determine parameters to reproduce the properties of the following three groups of systems:

(1)   The binary system $B_2O_3 + H_2O$, which encompasses the $H_3BO_3 + H_2O$ system in the composition range $0 < x_{B_2O_3} < 0.25$;
(2)   Binary aqueous solutions of metal borates and ternary systems of the type $B_2O_3 + M_nO + H_2O$ (where M = Na, Li ($n = 2$) or Ca, Mg ($n = 1$))
(3)   Mixtures of a metal borate or boric acid with a chloride salt or acid, i.e., $B + M + Cl + H + OH + H_2O$ systems, where M = Li, Na, and H

The model parameters have been first developed for the $B_2O_3 + H_2O$ binary, which includes the $H_3BO_3 + H_2O$ mixture in the full range to the melting point where $x_{H_3BO_3} = 1$. The boric acid–borate equilibria in aqueous solutions have also been analyzed to determine the standard partial molar properties of various aqueous boron species. These parameters provide a basis for modeling the properties of

metal borate systems (i.e., those from group 2 above), as the calculation of chemical and phase equilibria in these systems must be based on the same aqueous species and their properties. Modeling metal borate systems has led to introducing additional parameters that pertain to the specific nature of these systems (e.g., ion-pair formation and ion interactions involving the metal cation or the ion pair). These parameters, together with those determined in the first step, are then used to develop the model for mixtures of metal borates with chloride salts or hydrochloric acid.

RESULTS AND DISCUSSION

The binary system B_2O_3 + H_2O and the boric acid–borate equilibria in aqueous solutions

Extensive solubility data are available in the literature for the B_2O_3 + H_2O system [27–35], with three data sets covering the full composition range of the H_3BO_3 + H_2O subsystem [31,32,36]. These data extend to high temperatures, approaching the melting point of B_2O_3 [32,36]. Additional data are reported for volatilities and boiling points [33,37,38], equilibrium quotients [2,4], pH [39,40], and partial molar volumes and heat capacities [1,41–45] of boric acid solutions. As shown in Table 1, the literature data for this system cover wide ranges of temperature, pressure, and composition, and provide a comprehensive foundation for the determination of model parameters.

Boric acid is a weak Lewis acid. Instead of being a proton donor that dissociates in aqueous solutions, boric acid is a base acceptor and can interact with water to form $B(OH)_4^-$ and H^+, with an equilibrium constant (K_a) of only ~$6 \cdot 10^{-10}$ mol·L^{-1} at 25 °C [46]

$$H_3BO_{3(aq)} + H_2O = B(OH)_4^- + H^+ \qquad (9)$$

The presence of $H_3BO_{3(aq)}$ and $B(OH)_4^-$ has been confirmed by spectroscopic techniques [47]. The aqueous solution of boric acid also exhibits complex chemical equilibria involving various polyborate anions. The formation of polymeric borate ions in boric acid–borate solutions is well recognized. However, the identity of these ions has been a subject of research for many years. Experimental studies such as potentiometric titration, infrared and ion-exchange analysis, cryoscopic measurements, NMR, Raman, and vibrational spectroscopy have identified a number of polyborate species that vary with the solution pH and boron concentration [47]. Discrepancies exist between polymeric borate ions that have been identified by different authors and/or via different experimental methods. In the current study, a boric acid–borate equilibrium scheme has been selected to include the following species: $H_3BO_{3(aq)}$, $B(OH)_4^-$, $B_2O(OH)_5^-$, $B_3O_3(OH)_4^-$, $B_4O_5(OH)_4^{-2}$, and $B_5O_6(OH)_6^{-3}$, i.e.

$$H_3BO_{3(aq)} + 2H_2O = B(OH)_4^- + H_3O^+ \qquad (10a)$$

$$2H_3BO_{3(aq)} + H_2O = B_2O(OH)_5^- + H_3O^+ \qquad (10b)$$

$$3H_3BO_{3(aq)} = B_3O_3(OH)_4^- + H_3O^+ + H_2O \qquad (10c)$$

$$4H_3BO_{3(aq)} = B_4O_5(OH)_4^{-2} + 2H_3O^+ + H_2O \qquad (10d)$$

$$5H_3BO_{3(aq)} = B_5O_6(OH)_6^{-3} + 3H_3O^+ \qquad (10e)$$
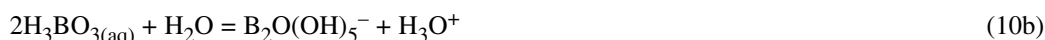
This equilibrium scheme is somewhat different from those used by Mesmer et al. [4] and Palmer et al. [2] in their studies of boric acid hydrolysis. The scheme (10a–e) can be reconciled with those of Mesmer et al. and Palmer et al. by adding appropriate numbers of moles of H_2O, for which thermodynamic properties are well known [48]. The comprehensive equilibrium quotient data from Mesmer et al. [4], as reviewed by Palmer et al. [2], and the limiting molar heat capacity and volumetric data from Hnedkovsky et al. [44], Ganopolsky et al. [43], Corti et al. [1], Ward and Millero [49], Abdulgatov and Azizov [41], and Ellis and McFadden [50] as well as the pH data from Macdonald et al. [39,40] have

been used as the primary sources to determine the values of $\Delta \bar{G}^{\circ}_f$, $\bar{S}^{\circ}$, and HKF parameters for the various aqueous borate species.

Speciation analysis of the boric acid + water system indicates a marginal amount of ionic species in the solution, due to the weak Lewis acid properties. Thus, as the boron concentration increases, the solution nonideality of the $H_3BO_3 + H_2O$ system can be primarily attributed to the effect of interactions between the predominant neutral molecules, i.e., H_2O and $H_3BO_3(aq)$. This binary system can exist as a liquid mixture over a wide range of compositions below the H_3BO_3 saturation concentration, ranging from pure liquid water to the melting point of the acid. There is thus no distinction between a solvent and a solute, as any one of the main components can be regarded as a "solute" or a "solvent" depending on the concentration. As the acid concentration changes from a dilute solution to a water-depleted region in the limit of molten B_2O_3, it is necessary to introduce species that can represent the loss of water molecules from H_3BO_3. Two monomeric neutral species, $HBO_{2(aq)}$ and $B_2O_{3(aq)}$, have been introduced for this purpose. These species have also been indicated by Kracek et al. [36] to exist in mixtures beyond the pure H_3BO_3 concentration. The chemical equilibria associated with these two species are

$$H_3BO_{3(aq)} = HBO_{2(aq)} + H_2O \tag{10f}$$

$$2H_3BO_{3(aq)} = B_2O_{3(aq)} + 3H_2O \tag{10g}$$

In the $H_3BO_3 + H_2O$ system, the solubility data that were measured at temperatures below 100 °C by different authors are in a good agreement. Above 100 °C, the results of Nasini and Ageno [33] show significantly higher solubilities than those of Benrath and McCulloch [31,32]. Also, the boiling point measurements of Nasini and Ageno give significantly lower values compared to those of von Stackelberg et al. [38]. The Nasini and Ageno data at $T > 100$ °C were thus excluded from the determination of model parameters. Solubility data beyond the limit of pure H_3BO_3 (i.e., for $x_{B_2O_3} \geq 0.25$) have been reported in the studies of McCulloch [32], von Stackelberg et al. [38], and Kracek et al. [36] in which all three solid phases $H_3BO_{3(s)}$, $HBO_{2(s)}$, and $B_2O_{3(s)}$ have been identified. Over this range of compositions, the melting points of $H_3BO_3(s)$ and $HBO_2(s)$ have been reported to be 170 and 203 °C, respectively [38], and the solubility of crystalline $B_2O_3(s)$ has been measured from 215 °C to its melting point (ca. 450~470 °C) [32,36]. These data have been included in the model development. Interaction parameters for two pairs of neutral species: $H_2O/H_3BO_{3(aq)}$ and $H_2O/HBO_{2(aq)}$ were introduced to represent the solution nonideality over the full concentration range, i.e., $x_{B_2O_3} = 0$~1. These parameters have been determined using the solubility and VLE data. The introduction of two neutral species, i.e., $HBO_{2(aq)}$ and $B_2O_{3(aq)}$, and the determination of interaction parameters for the $HBO_{2(aq)}/H_2O$ pair have enabled the model to reproduce the solubility behavior in the complete range of concentrations. Thermochemical properties (i.e., $\Delta \bar{G}^{\circ}_f$ and $\bar{S}^{\circ}$) for $HBO_{2(aq)}$ and $B_2O_{3(aq)}$ have been adjusted together with the activity coefficient interaction parameters. The standard-state thermochemical properties (i.e., ΔG°_f, S°, and C^0_p) of the solids $H_3BO_{3(s)}$ and $B_2O_{3(s)}$ have been taken from the literature [46,51], and those for $HBO_{2(s)}$ have been adjusted to fit the literature solubility data for this solid.

Table 5 summarizes the values of $\Delta \bar{G}^{\circ}_f$, $\bar{S}^{\circ}$, and HKF equation of state parameters for various aqueous boron species. Table 6 gives the Gibbs energy of formation, entropy, and heat capacity coefficients for various solid phases, and Table 7 summarizes the binary parameters in the virial interaction term (eqs. 4 and 5) that have been determined in this study.

Table 5 Standard partial molar Gibbs energy of formation, entropy, and parameters of the HKF equation of state [22–25] for standard partial molar thermodynamic properties $a_{HKF,1,...,4}$, $c_{HKF,1}$, $c_{HKF,2}$, ω for individual ionic and neutral boron species[a].

Species	$\Delta \bar{G}^\circ_f$ kJ·mol⁻¹	$\bar{S}^\circ$ J·mol⁻¹·K⁻¹	$a_{HKF,1}$	$a_{HKF,2}$	$a_{HKF,3}$	$a_{HKF,4}$	$c_{HKF,1}$	$c_{HKF,2}$	ω
$B_2O(OH)_5^-$	−1882.59	216.4256	−4.434878	13226.81	34.78676	0	11.02683	48925.48	0.1
$B_3O_3(OH)_4^-$	−2389.85	182.077	0.341374	0	107.2192	0	8.693543	74500.7	0.1
$B_4O_5(OH)_4^{-2}$	−3070.49	79.72733	1.192614	0	0	0	−57.1699	511476	0.1
$B_5O_6(OH)_6^{-3}$	−3978.53	86.81227	1.821451	0	0	0	−84.92186	327528	0.1
$B(OH)_4^-$	−1153.15	92.90074	−7.196197	21141.18	526.1382	−1430320	41.31961	−131414	76730.88
$B_2O_{3(aq)}$	−1193.63	77.91252	0	0	0	0	0	0	0
$H_3BO_{3(aq)}$	−968.674	157.3548	1.594831	−1116.716	−55.30091	108097	40.61506	−98866.36	5372.18
$HBO_{2(aq)}$	−720.176	74.25244	1.594831	−1116.716	−55.30091	108097	40.61506	−98866.36	5372.18
$NaB(OH)_{4(aq)}$[b]	−1416.62	164.0128	0.626	751.	2.8	−30900	73.5	189000	0
$LiB(OH)_{4(aq)}$[c]	−1440.70	196.9522	−7.19857	21134.28	537.7182	−1458080	58.78995	−137181	125351

[a]Parameters were determined in this study unless otherwise noted.
[b]Values were taken from Pokrovski et al. [54].
[c]$\Delta \bar{G}^\circ_f$ and $\bar{S}^\circ$ adjusted in this study, $a_{HKF,1,...,4}$, $c_{HKF,1}$, $c_{HKF,2}$, ω estimated using values for Li⁺ and $B(OH)_4^-$.

Table 6 Gibbs energy of formation, entropy, and heat capacity coefficients for solid phases.

Solid phase	$\Delta_f G°$ kJ·mol^{-1}	$S°$ J·mol^{-1}·K^{-1}	Cp (J·mol^{-1}·K^{-1}) = A + B/T + C/T^2 + DT^2 + ET^3				
			A	B	C	D	E
B_2O_3[a]	–1192.81	53.95	5.431501	0.272562	–377274	–2.52496E-4	9.76554E-8
H_3BO_3[a]	–968.937	88.74	13.2553	0.228299	0	0	0
HBO_2[b]	–724.532	36.373	179.5823	–0.477658	–3376930	7.19878E-4	–3.27844E-7
$Ca(OH)_2$[a]	–898.483	83.387	105.505	0.0124206	–1935890	0	0
$Ca_2B_6O_{11}·13H_2O$[c]	–8219.69	666.0928	737.2208	0	0	0	0
$Ca_2B_6O_{11}·9H_2O$[c]	–7276.65	108.2511	593.4036	0	0	0	0
$CaB_2O_4·4H_2O$[c]	–2886.98	125.52	263.979	0	0	0	0
$CaB_2O_4·6H_2O$[c]	–3363.49	340.827	343.979	0	0	0	0
$CaB_6O_{10}·4H_2O$[c]	–5367.90	230.1681	383.645	0	0	0	0
$Mg(OH)_2$[b]	–831.114	119.78	102.22	0.015107	–2617200	0	0
$MgB_2O_4·3H_2O$[c]	–2546.05	313.8	363.	0	0	0	0
$MgB_6O_{10}·7.5H_2O$[c]	–6087.43	385.4035	200.	0	0	0	0
$Mg_2B_6O_{11}·15H_2O$[c]	–8485.93	619.5425	630.	0	0	0	0
$LiOH$[b]	–441.908	40.5630	51.3812	0.032796	–1029300	0	0
$LiOH.H_2O$[b]	–682.953	73.4553	26.60817	0.177387	0	0	0
$LiBO_2$[b]	–962.032	74.22424	58.57098	0.046424	–1110220	5.64403E-6	–1.19606E-9
$LiB(OH)_4$[c]	–1447.33	91.3927	142	0	0	0	0
$Li_2B_4O_7·3H_2O$[c]	–3911.33	204.9339	364.9117	0	0	0	0
$LiB_5O_8·5H_2O$[c]	–4622.63	343.577	450.9565	0	0	0	0
$LiBO_2·8H_2O$[c]	–2873.42	317.1078	389.	0	0	0	0
$NaOH$[b]	–381.092	49.63312	–7.934	0.158243	1804000	0	0
$NaOH.H_2O$[b]	–629.654	100.2302	90.1234	0	0	0	0
$Na_2O·5B_2O_3·10H_2O$[c]	–9190.41	699.0376	786.51	0	0	0	0
$Na_2O·5B_2O_3·2H_2O$[c]	–7290.58	29.65925	451.79	0	0	0	0
$Na_2B_2O_4·H_2O$[c]	–2093.03	119.0239	168.11	0	0	0	0
$Na_2B_2O_4·4H_2O$[c]	–2821.96	261.7197	20.17787	0	0	0	0
$Na_2B_2O_4·8H_2O$[c]	–3775.00	492.6786	460.99	0	0	0	0
$Na_2B_4O_7·2H_2O$[c]	–3579.52	340.1408	270.41	0	0	0	0
$Na_2B_4O_7·4H_2O$[c]	–4082.37	225.8946	434.0544	0	0	0	0
$Na_2B_4O_7·5H_2O$[c]	–4317.43	322.8337	395.93	0	0	0	0
$Na_2B_4O_7·10H_2O$[c]	–5510.13	551.1332	605.13	0	0	0	0
$2Na_2O·B_2O_3·H_2O$[c]	–2615.55	67.13019	233.93	0	0	0	0
$2Na_2O·5B_2O_3·5H_2O$[c]	–8647.91	931.053	643.12	0	0	0	0
$2Na_2O·5.1B_2O_3·7H_2O$[c]	–9281.01	591.1657	732.85	0	0	0	0
$NaBO_2·NaCl·2H_2O$[c]	–1798.87	274.6414	197.69	0	0	0	0

[a]Values were from Chase [51], Wagman et al. [46], Johnston and Kerr [99].
[b]Values of $\Delta_f G°$ and $S°$ were adjusted in this study and those for Cp were from Chase [51], Stull et al. [100], Bauer et al. [101], Robie and Hemingway [102], and Glushko et al. [103]
[c]Values of $\Delta_f G°$ and $S°$ were adjusted; Cp coefficients were either adjusted or estimated [104] in this study.

Table 7 Binary parameters in the virial interaction term (eqs. 4 and 5) determined in this study for species pairs involving boron species.

| Species i	Species j	$b_{0,ij}$	$b_{1,ij}$	$b_{2,ij}$	$c_{0,ij}$	$c_{1,ij}$	$c_{2,ij}$
$H_3BO_{3(aq)}$	H_2O	0.2269030	0	–102.5526	0	0	0
$HBO_{2(aq)}$	H_2O	0	0	–548.2939	0	0	0
$HBO_{2(aq)}$	Li^+	–2.584525	–1.0559810E-03	2706.596	0	0	0
$H_3BO_{3(aq)}$	Li^+	–2.584525	–1.0559810E-03	2706.596	0	0	0
$B_3O_3(OH)_4^-$	Li^+	–2.584525	–1.0559810E-03	2706.596	0	0	0
$B_4O_5(OH)_4^{-2}$	Li^+	–2.584525	–1.0559810E-03	2706.596	0	0	0
$B_5O_6(OH)_6^{-3}$	Li^+	–2.584525	–1.0559810E-03	2706.596	0	0	0

(*continues on next page*)

Table 7 (Continued).

Species i	Species j	$b_{0,ij}$	$b_{1,ij}$	$b_{2,ij}$	$c_{0,ij}$	$c_{1,ij}$	$c_{2,ij}$
$B(OH)_4^-$	Li^+	–2.584525	–1.0559810E-03	2706.596	0	0	0
$B_2O(OH)_5^-$	Li^+	–2.584525	–1.0559810E-03	2706.596	0	0	0
$H_3BO_{3(aq)}$	Na^+	–98.41640	0.1118610	22208.42	–0.4351380	0	1251.747
$B_3O_3(OH)_4^-$	Na^+	–125.9094	0.1756280	24181.96	0	0	0
$B_4O_5(OH)_4^{-2}$	Na^+	–125.9094	0.1756280	24181.96	0	0	0
$B_5O_6(OH)_6^{-3}$	Na^+	–125.9094	0.1756280	24181.96	0	0	0
$B(OH)_4^-$	Na^+	503.7248	–0.5207550	–117766.1	0	0	0
$NaB(OH)_{4(aq)}$	OH^-	133.4344	–0.2064430	–19594.48	–160.2999	0.2610480	19668.85
$NaB(OH)_{4(aq)}$	Na^+	133.4344	–0.2064430	–19594.48	–160.2999	0.2610480	19668.85
$NaB(OH)_{4(aq)}$	$H_3BO_{3(aq)}$	–98.41640	0.1118610	22208.42	–0.4351380	0	1251.747
$NaB(OH)_{4(aq)}$	$B(OH)_4^-$	503.7248	–0.5207550	–117766.1	0	0	0
$NaB(OH)_{4(aq)}$	$B_3O_3(OH)_4^-$	0	0	3096.541	0	0	0
$NaB(OH)_{4(aq)}$	$B_4O_5(OH)_4^{-2}$	0	0	3096.541	0	0	0
$NaB(OH)_{4(aq)}$	$B_5O_6(OH)_6^{-3}$	0	0	3096.541	0	0	0
$H_3BO_{3(aq)}$	Mg^{2+}	0	0	5370.074	0	0	0
$H_3BO_{3(aq)}$	Ca^{+2}	20.66380	0	0	0	0	0
$H_3BO_{3(aq)}$	$CaOH^+$	20.66380	0	0	0	0	0
$B(OH)_4^-$	Ca^{2+}	–3586.026	0	1048070.	0	0	0
$B(OH)_4^-$	$CaOH^+$	–3586.026	0	1048070.	0	0	0
$HBO_{2(aq)}$	Cl^-	–71.20732	0	18893.75	0	0	0
$H_3BO_{3(aq)}$	Cl^-	24.76295	0	–11483.88	0	0	0
$B_2O(OH)_5^-$	Cl^-	29.12929	0	–9823.521	0	0	0
$B_3O_3(OH)_4^-$	Cl^-	29.12929	0	–9823.521	0	0	0
$B_4O_5(OH)_4^{-2}$	Cl^-	29.12929	0	–9823.521	0	0	0
$B_5O_6(OH)_6^{-3}$	Cl^-	29.12929	0	–9823.521	0	0	0
$NaB(OH)_{4(aq)}$	Cl^-	–0.7870918	0	250.6625	0	0	0
$H_3BO_{3(aq)}$	H_3O^+	8.331318	0	0	0	0	0

　　　Using the model parameters listed in Tables 5–7, the solubilities in the $B_2O_3 + H_2O$ system have been accurately reproduced. This is shown in Figs. 1 and 2 where the calculated and experimental results are compared in the full composition range. In Fig. 1, the solubilities in the $H_3BO_3 + H_2O$ system are illustrated in the full range, i.e., $x_{H_3BO_3} = 0$ to 1. The x-axis is presented as $x_{H_3BO_3}^{0.5}$ to emphasize the details in the low boric acid concentration range (i.e., for $x_{H_3BO_3} < 0.01$). Results in the full composition range of the $B_2O_3 + H_2O$ system are shown in Fig. 2, which also includes the system $H_3BO_3 + H_2O$ in the $0 \le x_{B_2O_3} \le 0.25$ range. The model also reproduces VLE data for aqueous boric acid as represented by the volatility K (y/x) and boiling points as functions of temperature and acid concentration. These results are shown in Fig 3. The speciation results are depicted in Fig. 4 in the form of a plot of pH as a function of temperature at various boric acid concentrations. This confirms the correctness of the thermochemical properties of aqueous neutral and ionic species, which are necessary for chemical equilibrium calculations. All these results show that the MSE model accurately reproduces experimental data of various types in the full concentration range of the $B_2O_3 + H_2O$ system.

　　　The model parameters developed for the $B_2O_3 + H_2O$ system provide a basis for modeling metal borate systems in the presence or absence of H_3BO_3 and other salts, acids, and bases. This will be discussed in the following sections.
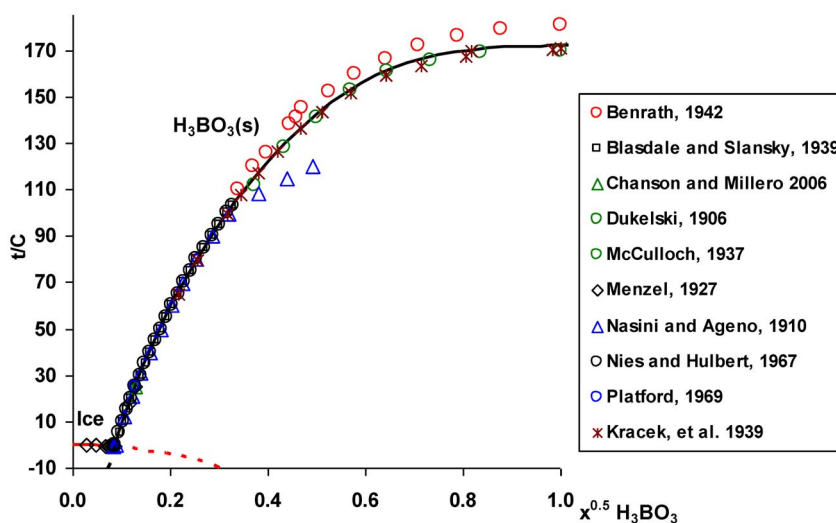
Fig. 1 Solubility of boric acid in water as a function of temperature. The symbols are experimental data from the literature, and the lines are calculated using the MSE model. The dashed lines represent metastable phases of H_3BO_3(s) and ice.
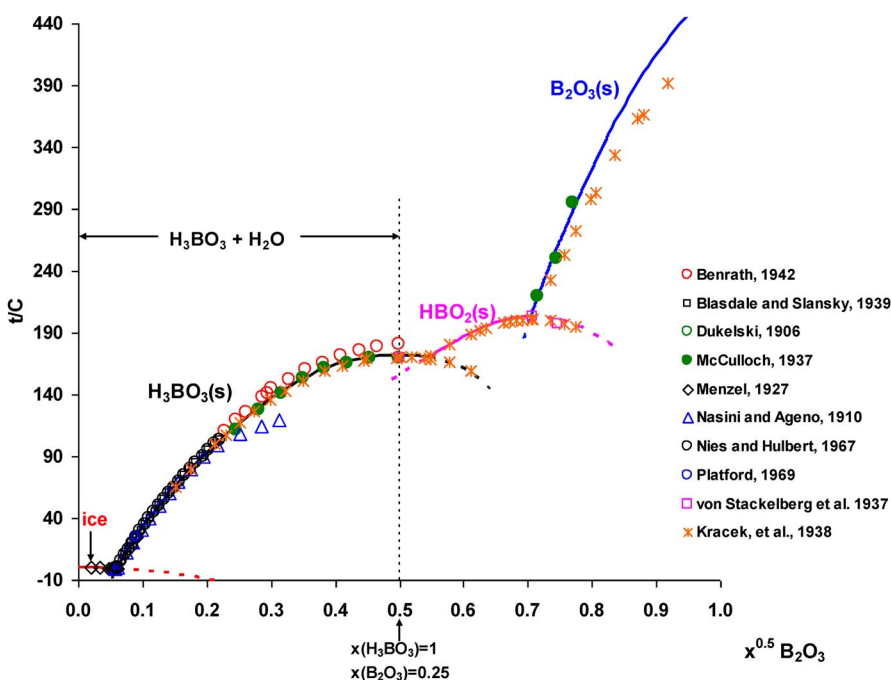
Fig. 2 Solubility in the B_2O_3 + H_2O system as a function of temperature. The symbols are experimental data from the literature, and the lines are calculated using the MSE model. The dashed lines represent metastable solid phases.

(a)　　　　　　　　　　　　　　　　　　　(b)
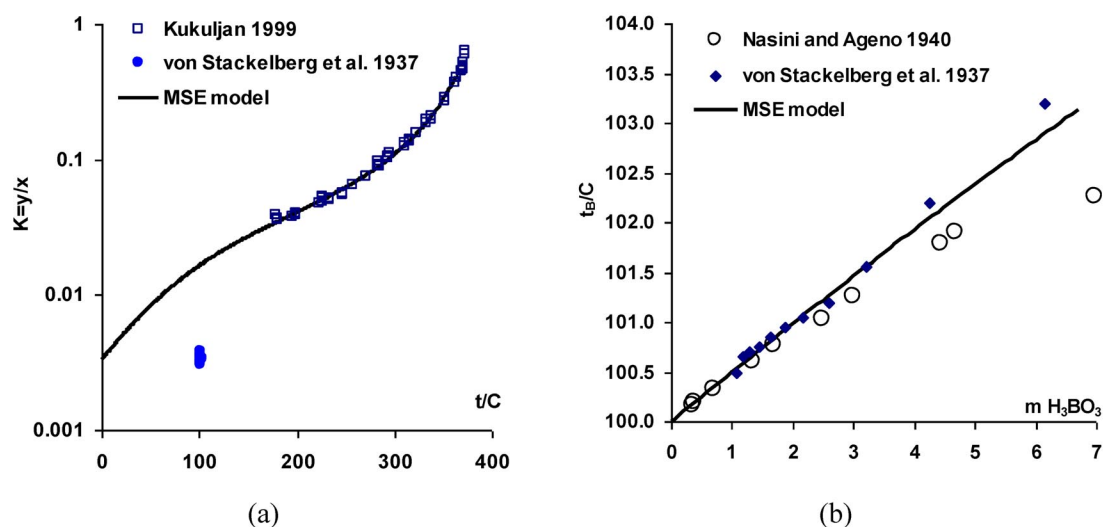
Fig. 3 VLE results for the H_3BO_3 + H_2O system: (a) volatility as a function of temperature and (b) boiling points as a function of boric acid concentration. The symbols denote literature data, and the lines are calculated using the MSE model.
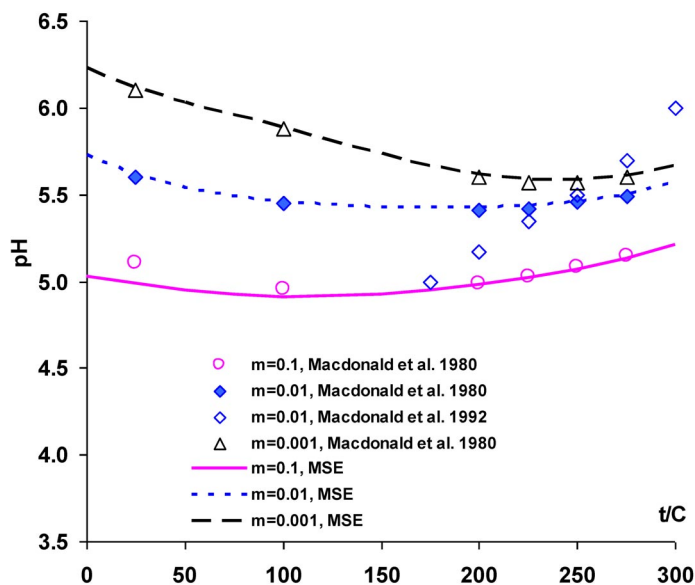
Fig. 4 Calculated and experimental pH in boric acid solutions as a function of temperature and the concentration of H_3BO_3. The symbols are literature data, and the lines are calculated using the MSE model.

Metal borate systems

These systems include aqueous binary metal borates, e.g., (Li or Na)$_2B_4O_7$ + H_2O, (Li or Na)BO_2 + H_2O, ternary systems H_3BO_3 + $M(OH)_n$ + H_2O, and aqueous M-borates in the presence of excess amounts of H_3BO_3 or $M(OH)_n$, where M = Na, Li (n = 1) or Ca, Mg (n = 2). These binary and ternary systems are grouped together in the determination of model parameters, as the prevailing aqueous species can be the same in the binary and ternary systems and, subsequently, the introduced binary

interaction parameters may affect both the binary and ternary systems. A simultaneous regression of data for these systems ensures the accuracy of the model parameters. The literature data that were used in model development for these systems are summarized in Tables 2 and 3.

For the Li and Na borate solutions, the formation of ion pairs $Na^+B(OH)_4^-{}_{(aq)}$ and $Li^+B(OH)_4^-{}_{(aq)}$ has been experimentally identified and their stability constants have been reported on the basis of electrical conductivity, UV–vis spectrophotometric and electromagnetic field (EMF) measurements [52–56]. The standard thermochemical properties for $Na^+B(OH)_4^-{}_{(aq)}$ have been adopted from Pokrovski et al. [54]. For $Li^+B(OH)_4^-{}_{(aq)}$, there are no reported values of the HKF parameters in the literature. Thus, the values of $a_{HKF,1,...4}$, $c_{HKF,1}$, $c_{HKF,2}$, and ω for this ion pair have been estimated based on those of aqueous Li^+ and $B(OH)_4^-$ ions. Further, the standard partial molar Gibbs energy ($\Delta\bar{G}°_f$) and entropy ($\bar{S}°$) were adjusted, together with other model parameters, based on primary experimental data. The formation of similar ion pairs between borate and alkaline-earth metal ions has also been reported in the literature [57]. The reported stability constants for these ion pairs are somewhat lower than that for $Na^+B(OH)_4^-{}_{(aq)}$. The concentration ranges with respect to Mg and Ca in the corresponding borate solutions are significantly narrower compared to those for the Li and Na systems, which allows us to neglect ion-pair formation in the Mg and Ca systems.

For each of these metal borate systems, multiple solid phases exist, depending on the temperature and the concentrations of the base, metal borate or boric acid. For example, the following solid phases have been reported in experimental solubility studies of sodium borate systems: $Na_2B_2O_4\cdot H_2O$, $Na_2B_2O_4\cdot 4H_2O$, $Na_2B_2O_4\cdot 8H_2O$, $Na_2B_4O_7\cdot 2H_2O$, $Na_2B_4O_7\cdot 4H_2O$, $Na_2B_4O_7\cdot 5H_2O$, $Na_2B_4O_7\cdot 10H_2O$, $Na_2O\cdot 5B_2O_3\cdot 2H_2O$, $Na_2O\cdot 5B_2O_3\cdot 10H_2O$, $2Na_2O\cdot B_2O_3\cdot H_2O$, $2Na_2O\cdot 5B_2O_3\cdot 5H_2O$, and $2Na_2O\cdot 5.1B_2O_3\cdot 7H_2O$. The reported solid lithium borate phases include: $LiBO_2$, $LiB(OH)_4$ (or $LiBO_2\cdot 2H_2O$), $LiBO_2\cdot 8H_2O$, $Li_2B_4O_7\cdot 3H_2O$, and $LiB_5O_8\cdot 5H_2O$. For the magnesium and calcium borate systems, the solid phases that were identified in solubility measurements include: $CaB_2O_4\cdot 4H_2O$, $CaB_2O_4\cdot 6H_2O$, $CaB_6O_{10}\cdot 4H_2O$, $Ca_2B_6O_{11}\cdot 9H_2O$, $Ca_2B_6O_{11}\cdot 13H_2O$, $MgB_2O_4\cdot 3H_2O$, $MgB_6O_{10}\cdot 7.5H_2O$, and $Mg_2B_6O_{11}\cdot 15H_2O$. Thermochemical properties for all solid phases that were used for calculating solubilities are collected in Table 6. In addition to the metal borates and their hydrates, the properties of the hydroxides of Li, Na, Ca, and Mg are also listed in this table, as these solid phases can precipitate at high hydroxide concentrations in each of the $H_3BO_3 + M(OH)_n + H_2O$ systems. Solubility data for other solids, especially the unhydrated metal borates such as $NaBO_2$, $Na_2B_4O_7$, $Li_2B_4O_7$, LiB_3O_5, $Li_2B_8O_{13}$, CaB_2O_4, and MgB_2O_4, have not been found in the literature although their thermochemical properties have been reported [46,51,58–60]. Such anhydrous solid phases exist only at high temperatures at which either no sufficient information can be found for model development or their stability ranges fall beyond the validity range of the MSE model. Such solid phases have not been included in the analysis in the present study. However, their thermochemical properties from the literature have been examined to ensure that these phases do not precipitate in the regions where other solid phases are stable.

In addition to the multiple solid phases that can be in equilibrium with the solution under varying conditions, the chemistry of the metal borate systems is typically complicated by strong speciation effects due to the chemical equilibria between various aqueous mono- and polyborate neutral and ionic species, which are strongly dependent on the solution pH, concentration, and temperature. Thus, the model for these systems has been developed based on the analysis of experimental data (Tables 2 and 3) and by taking into account the chemical speciation effects. The reported metastable solubilities for a number of solids (i.e., in supersaturated solutions) have also been taken into consideration in the model development to ensure an appropriate extrapolation of solubilities. Moreover, metastable equilibria in concentrated salt solutions are important for understanding evaporation processes in the exploitation of salt lake brines and for applications in crystallization.

In modeling highly speciated systems at high concentrations, it is vitally important to select appropriate species pairs for which interaction parameters should be introduced to represent solution nonideality. This can be especially challenging for solutions containing multiple mono- and polymeric

species whose distribution can vary with conditions such as temperature, pH, and the total concentrations of the elements. In such cases, there can be a large number of pairs of species that may be possibly considered. To address this problem, the introduction of pair interactions in the process of model development was based on the analysis of the speciation results. In general, the interaction parameters are introduced only for the species pairs that are present in a sufficient amount to contribute to the solution's nonideal behavior. Due to the differences in the distribution of boron species as a function of system conditions, these species may all be expected to affect phase equilibria under various conditions at which they predominate and interact with other species such as cations or ion pairs that are also present at a significant level. In this study, we assume that various borate species, neutral or anionic, may interact with cations (i.e., Na^+ or Li^+) in a similar way. This assumption allows the interactions between a cation and several borate species to be set equal to each other in the process of parameter fitting. Likewise, interactions between a borate species and various other species, such as a cation and its complexes, may also be assumed to be the same. This constraint significantly reduces the number of adjustable parameters.

The binary interaction parameters that have been determined for the borate systems are collected in Table 7. For the $MgO + B_2O_3 + H_2O$ and $CaO + B_2O_3 + H_2O$ systems, the equilibrium concentrations in saturated solutions are relatively low compared to those in the $Li_2O + B_2O_3 + H_2O$ and $Na_2O + B_2O_3 + H_2O$ systems. Therefore, only the interaction parameters between a cation (i.e., Ca^{+2}, Mg^{+2}, or $CaOH^+$) and a monoborate species (i.e., $H_3BO_{3(aq)}$ or $B(OH)_4^-$) are necessary to reproduce the solubility behavior in these systems. In addition to the interaction parameters listed in Table 7, parameters have also been determined for the $LiOH + H_2O$ and $NaOH + H_2O$ systems to provide a foundation for modeling the Li and Na borates in the presence of LiOH and NaOH. These parameters are listed in Table 8.

Results of modeling the metal borate systems are shown in Figs. 5–10. The model results have been calculated using the parameters listed in Tables 5–8. In Fig. 5, the results for the solubilities in the $NaBO_2 + H_2O$ and $LiBO_2 + H_2O$ systems are shown. Multiple metaborates and/or their hydrates with varying hydration numbers can precipitate as the temperature changes. The solubilities of lithium metaborate and its hydrates are significantly lower than those of the corresponding sodium metaborates, indicating bigger differences in the total hydration energy for the aqueous Na^+ and borate ions and the lattice energy for the sodium borate solids compared to those in the lithium borate system. Since the MSE model is self-consistent and its parameters have been determined using multiple thermodynamic properties, it simultaneously reproduces the pH and VLE data in aqueous metal borate systems. Figure 6 compares the calculated and experimental pH values for the aqueous solutions of $NaBO_2$, $Na_2B_4O_7$, and $NaBO_2 \cdot 2B_2O_3 \cdot 2H_2O$ at 20 °C, and the vapor pressures in the $NaBO_2 + H_2O$ system at various temperatures.

Phase behavior is exceedingly complex for all of the metal borate ternary systems studied here. Figure 7 presents the results for the $LiOH + H_3BO_3 + H_2O$ system at various temperatures. To better illustrate the phase behavior at low concentrations, the solubilities have been plotted as the square root of the molalities, $m^{0.5}$, for both LiOH and H_3BO_3. The results show that a total of 8 solid phases precipitate over the temperature range 10~100 °C: $H_3BO_3(s)$, $Li_2B_4O_7 \cdot 3H_2O$, $LiBO_2 \cdot 8H_2O$, $LiB(OH)_4$, $LiB_5O_8 \cdot 5H_2O$, $LiBO_2(s)$, $LiOH \cdot H_2O$, and LiOH. The solubilities increase with temperature and three solid phases, i.e., $LiOH \cdot H_2O$, $Li_2B_4O_7 \cdot 3H_2O$, and $H_3BO_3(s)$ precipitate at all temperatures studied. At relatively low temperatures (i.e., below 40 °C), $LiBO_2 \cdot 8H_2O$ can precipitate over a wide LiOH concentration range at relatively low H_3BO_3 concentrations. The solid phase $LiB(OH)_4$ starts to precipitate as the temperature increases to ca. 30 °C at moderate to high LiOH concentrations (e.g., 1.6~6.1 m at 40 °C and 2.5~8.3 m at 80 °C) and at the molar ratio Li/B greater than 1. A solid phase, $LiB_5O_8 \cdot 5H_2O$, forms at 80 °C or higher temperatures at very high H_3BO_3 concentrations (i.e., 18~19 m at 80 °C and 31–33 m at 100 °C) and at a molar ratio B/Li~5. The unhydrated phase $LiBO_2(s)$ is observed only at 100 °C and at high LiOH concentrations (e.g., for LiOH ≈ 7.7~10.7 m). The stability range of the solid

Table 8 Binary parameters in the virial interaction term (eqs. 4 and 5) determined in this study for species pairs in the LiOH + H$_2$O and NaOH + H$_2$O systems.

Species i	Species j	Interaction parameters	
H$_2$O	LiOH$_{(aq)}$	$b_{2,ij}$	−1088.296
OH⁻	Li⁺	$b_{0,ij}$, $b_{1,ij}$, $b_{2,ij}$, $b_{3,ij}$, $c_{0,ij}$, $c_{1,ij}$, $c_{2,ij}$	−65.93330, 0.2890020, 550.5028, −4.5257500E-04, −154.1532, 0.3208480, 26183.13
H$_2$O	NaOH$_{(aq)}$	$b_{0,ij}$, $b_{1,ij}$, $b_{2,ij}$	13.16820, −1.252222E-02, −2316.810
OH⁻	Na⁺	$b_{0,ij}$, $b_{1,ij}$, $b_{2,ij}$, $b_{5,ij}$, $b_{6,ij}$, $b_{7,ij}$, $b_{8,ij}$, $b_{9,ij}$, $b_{p2,ij}$, $c_{0,ij}$, $c_{1,ij}$, $c_{2,ij}$, $c_{5,ij}$, $c_{6,ij}$, $c_{7,ij}$, $c_{8,ij}$, $c_{9,ij}$	−223.7240, 2.867730, 568.5530, −1.2007400E-06, 2.6586300E-02, −0.3974260, −73972.00, 3.39350E-02, −1.138020 455.3660, −5.726060, −14362.30, 2.26640E-06, 2.65863E-02, 0.797161, 138833.0, 3.3935000E-02
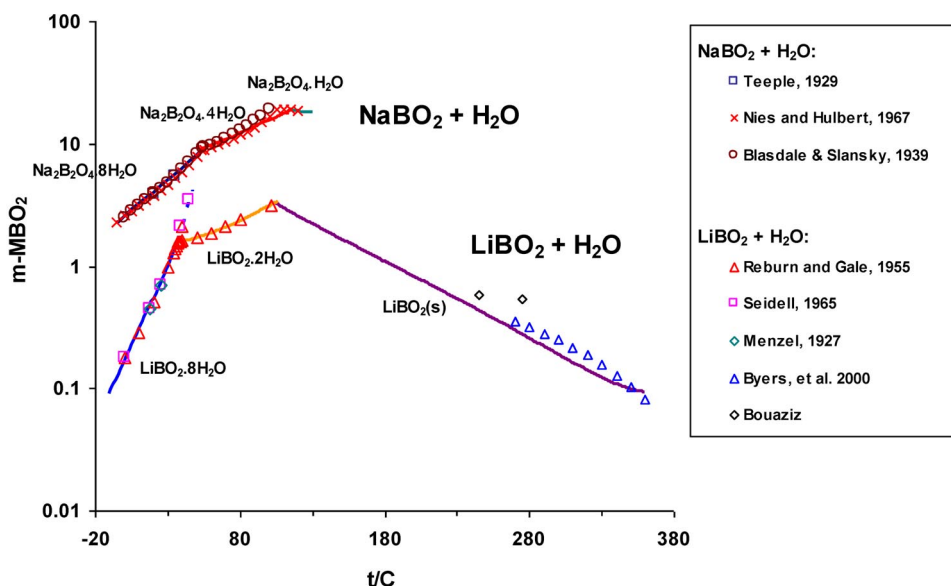
Fig. 5 Solubilities in the $NaBO_2$ + H_2O and $LiBO_2$ + H_2O systems. The symbols denote literature data, and the lines are calculated using the MSE model.

(a)

(b)
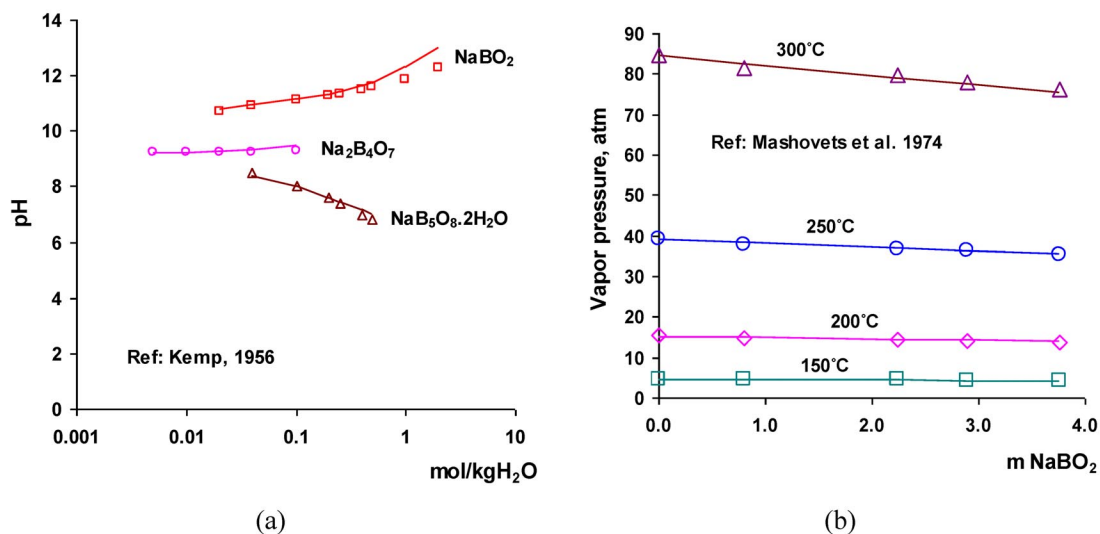
Fig. 6 Properties of sodium borate solutions: (a) pH of aqueous solutions of $NaBO_2$, $Na_2B_4O_7$, and $NaBO_2 \cdot 2B_2O_3 \cdot 2H_2O$; (b) vapor pressures in the $NaBO_2$ + H_2O system at temperatures from 150 to 300 °C. The symbols are literature data, and the lines are calculated using the MSE model.
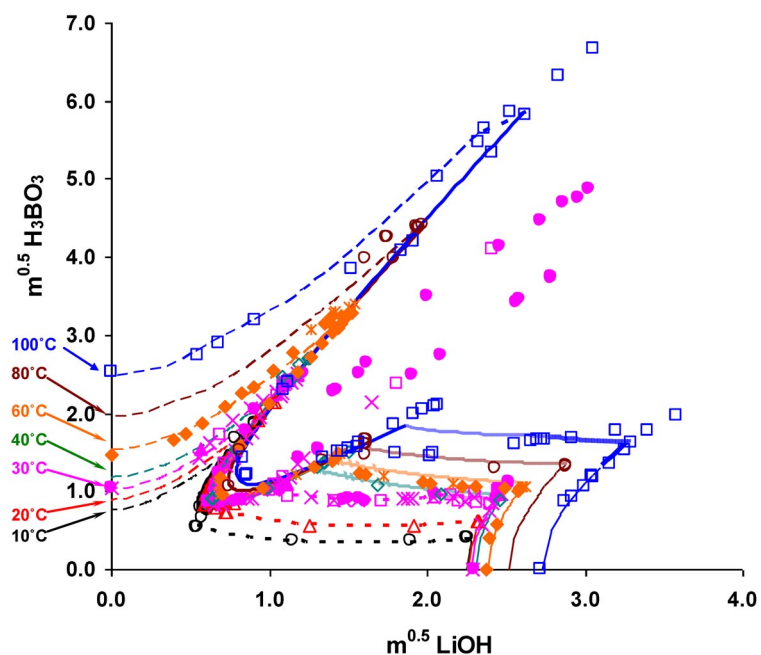
Fig. 7 Solubilities in the LiOH + H$_3$BO$_3$ + H$_2$O system at various temperatures. The symbols are literature data, and the lines are calculated using the MSE model:

○ 10 °C, Reburn and Gale, 1955	— 40 °C, MSE: Li$_2$B$_4$O$_7$·3H$_2$O
— 10 °C, MSE: LiOH·1H$_2$O	–– 40 °C, MSE: H$_3$BO$_3$(s)
..... 10 °C, MSE: LiBO$_2$·8H$_2$O	◆ 56 °C, Bouaziz, 1961
— 10 °C, MSE: Li$_2$B$_4$O$_7$·3H$_2$O	✳ 60 °C, Reburn and Gale, 1955
–– 10 °C, MSE: H$_3$BO$_3$(s)	— 60 °C, MSE: LiOH·1H$_2$O
△ 20 °C, Reburn and Gale, 1955	— 60 °C, MSE: LiB(OH)$_4$(s)
— 20 °C, MSE: LiOH·1H$_2$O	— 60 °C, MSE: Li$_2$B$_4$O$_7$·3H$_2$O
..... 20 °C, MSE: LiBO$_2$·8H$_2$O	–– 60 °C, MSE: H$_3$BO$_3$(s)
— 20 °C, MSE: Li$_2$B$_4$O$_7$·3H$_2$O	○ 80 °C, Reburn and Gale, 1955
–– 20 °C, MSE: H$_3$BO$_3$(s)	— 80 °C, MSE: LiOH·1H$_2$O
□ 30 °C, Reburn and Gale, 1955	— 80 °C, MSE: LiB(OH)$_4$(s)
▲ 30 °C, Rollet and Bouaziz, 1955	— 80 °C, MSE: Li$_2$B$_4$O$_7$·3H$_2$O
● 30 °C, Dukelski, 1906	--- 80 °C, MSE: LiB$_5$O$_8$·5H$_2$O
✕ 30 °C, Bouaziz, 1961	–– 80 °C, MSE: H$_3$BO$_3$(s)
— 30 °C, MSE: LiOH·1H$_2$O	□ 100 °C, Bouaziz, 1961
— 30 °C, MSE: LiB(OH)$_4$(s)	— 100 °C, MSE: LiOH·1H$_2$O
..... 30 °C, MSE: LiBO$_2$·8H$_2$O	━ 100 °C, MSE: LiOH(s)
— 30 °C, MSE: Li$_2$B$_4$O$_7$·3H$_2$O	— 100 °C, MSE: LiBO$_2$(s)
–– 30 °C, MSE: H$_3$BO$_3$(s)	— 100 °C, MSE: LiB(OH)$_4$(s)
◇ 40 °C, Reburn and Gale, 1955	— 100 °C, MSE: Li$_2$B$_4$O$_7$·3H$_2$O
— 40 °C, MSE: LiOH·1H$_2$O	--- 100 °C, MSE: LiB$_5$O$_8$·5H$_2$O
— 40 °C, MSE: LiB(OH)$_4$(s)	–– 100 °C, MSE: H$_3$BO$_3$(s)
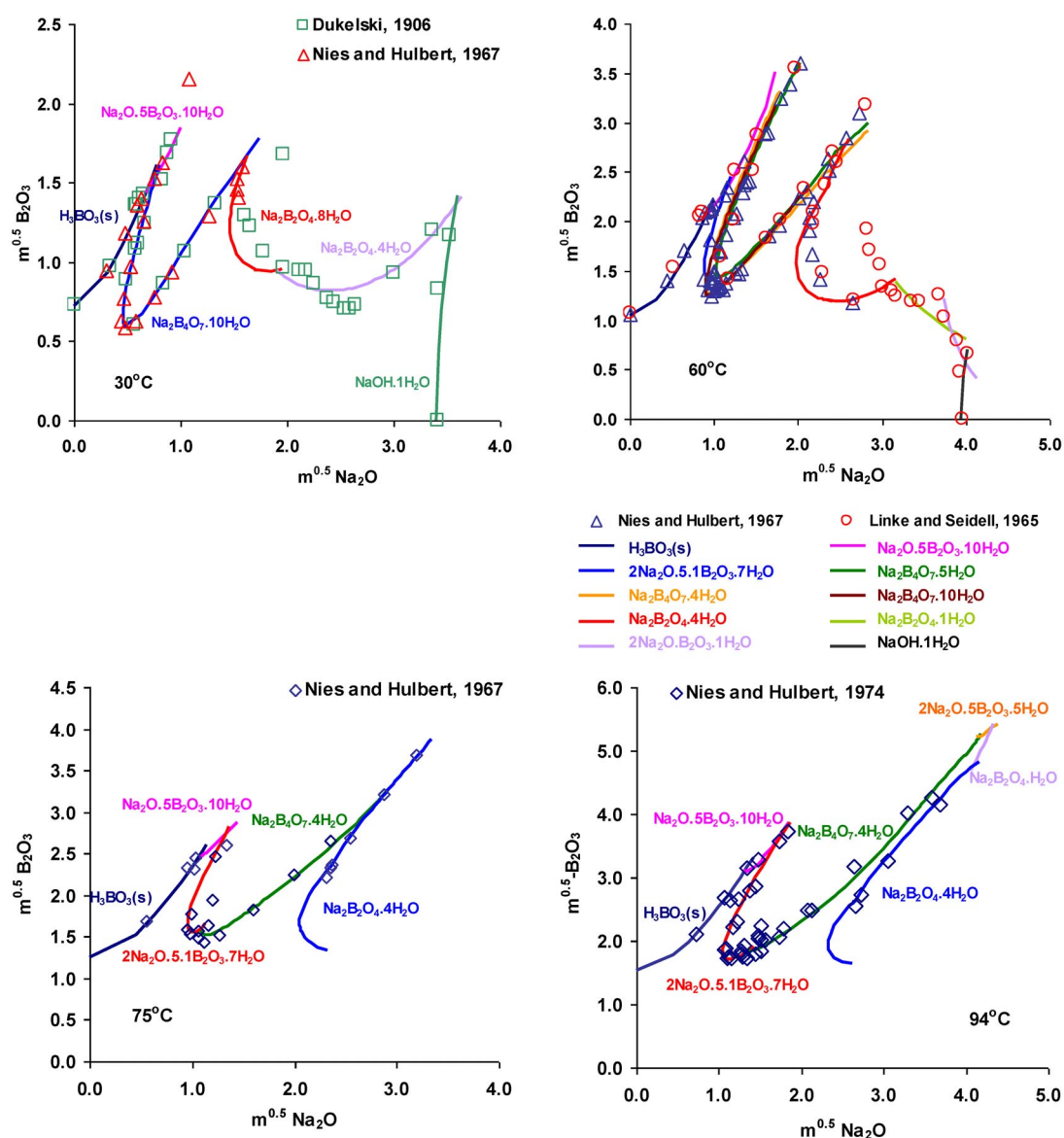
Fig. 8 Solubilities in the $Na_2O + B_2O_3 + H_2O$ system at various temperatures. The symbols are literature data, and the lines are calculated using the MSE model.

$H_3BO_3(s)$ increases as the temperature rises. This solid can precipitate at a LiOH concentration as high as 5.4 m at 100 °C at high ratios of B/Li (i.e., B/Li ≥ 5.8 at 100 °C). The complex phase behavior of this system is accurately represented by the MSE model. The points that have not been reproduced at 30 °C come from the early work of Dukelski (1906) [29] and can be attributed to the formation of metastable solid phases and supersaturation effects as indicated by Reburn and Gale [61].

Similar phase behavior is shown for other $M_nO + B_2O_3 + H_2O$ systems, where M = Na, Mg, and Ca. Figures 8–10 show the solubilities at various temperatures for the $Na_2O + B_2O_3 + H_2O$, MgO + $B_2O_3 + H_2O$, and CaO + $B_2O_3 + H_2O$ systems, respectively. The J-shaped curves, which were observed in the $Li_2O + B_2O_3 + H_2O$ system saturated with $Li_2B_4O_7 \cdot 3H_2O$, are also displayed by the saturation
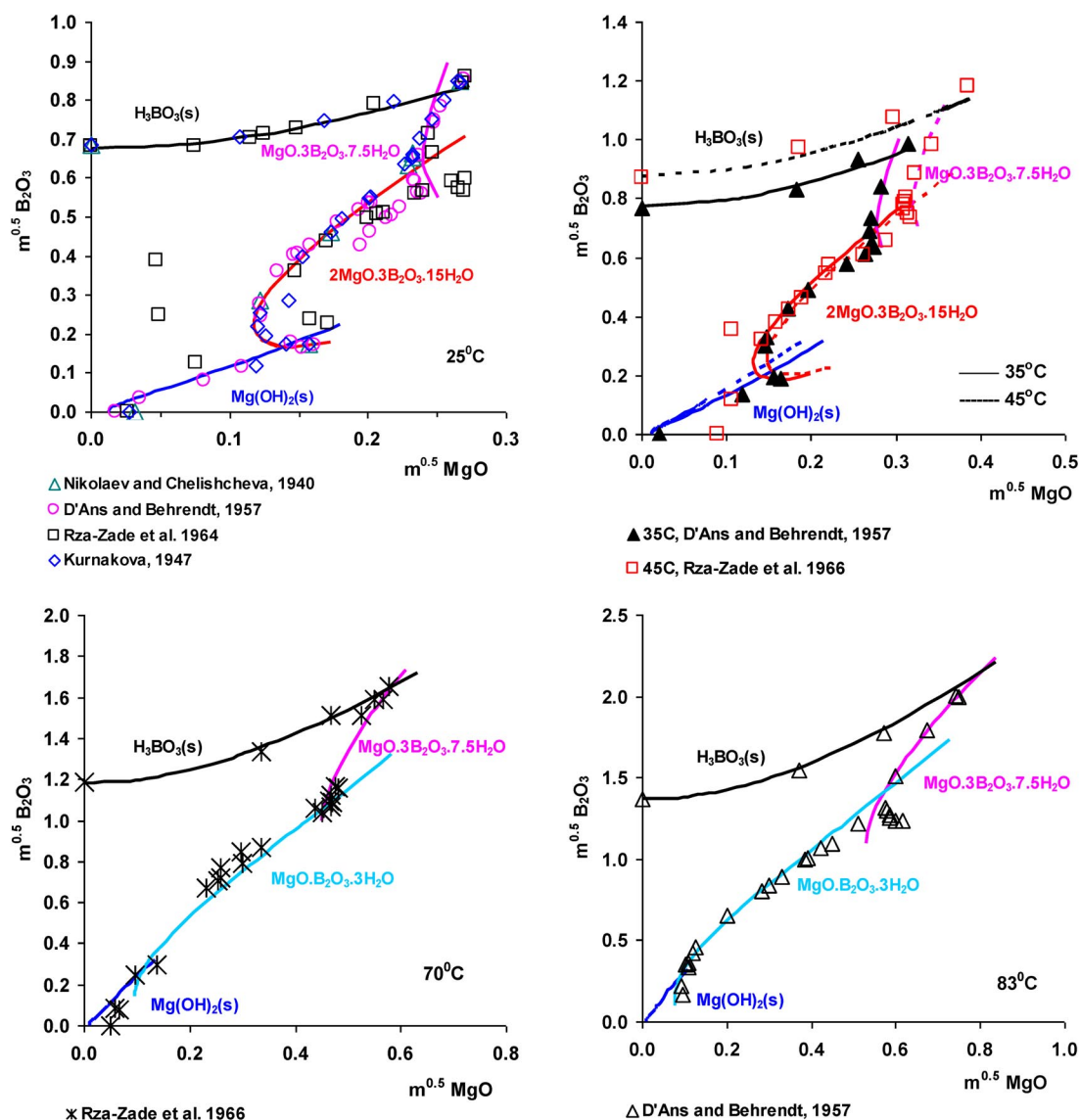
Fig. 9 Solubilities in the MgO + B$_2$O$_3$ + H$_2$O system at various temperatures. The symbols are literature data, and the lines are calculated using the MSE model.

curves of Na$_2$B$_4$O$_7$·10H$_2$O and several other solids in the Na$_2$O + B$_2$O$_3$ + H$_2$O system, and by those of Mg$_2$B$_6$O$_{11}$·15H$_2$O and Ca$_2$B$_6$O$_{11}$·nH$_2$O (n = 9 and 11) in the MgO + B$_2$O$_3$ + H$_2$O and CaO + B$_2$O$_3$ + H$_2$O systems, respectively. For the Na$_2$O + B$_2$O$_3$ + H$_2$O system, the model includes a total of 12 hydrates of various sodium borates and double salts, in addition to H$_3$BO$_3$(s) at relatively low NaOH concentrations and NaOH·nH$_2$O in highly concentrated alkaline solutions. As shown in Fig. 8, more than one of such J-shaped curves can appear in this system at a single temperature and multiple stable and metastable solid phases can precipitate (c.f. the results at 60 °C). The complex solubility behavior, together with the strong chemical speciation effects as discussed earlier, makes it challenging to model phase equilibria in these systems. As shown in Figs. 5–10, the MSE model is capable of representing these complex phase equilibrium patterns with a good accuracy for all of the ternary mixtures.
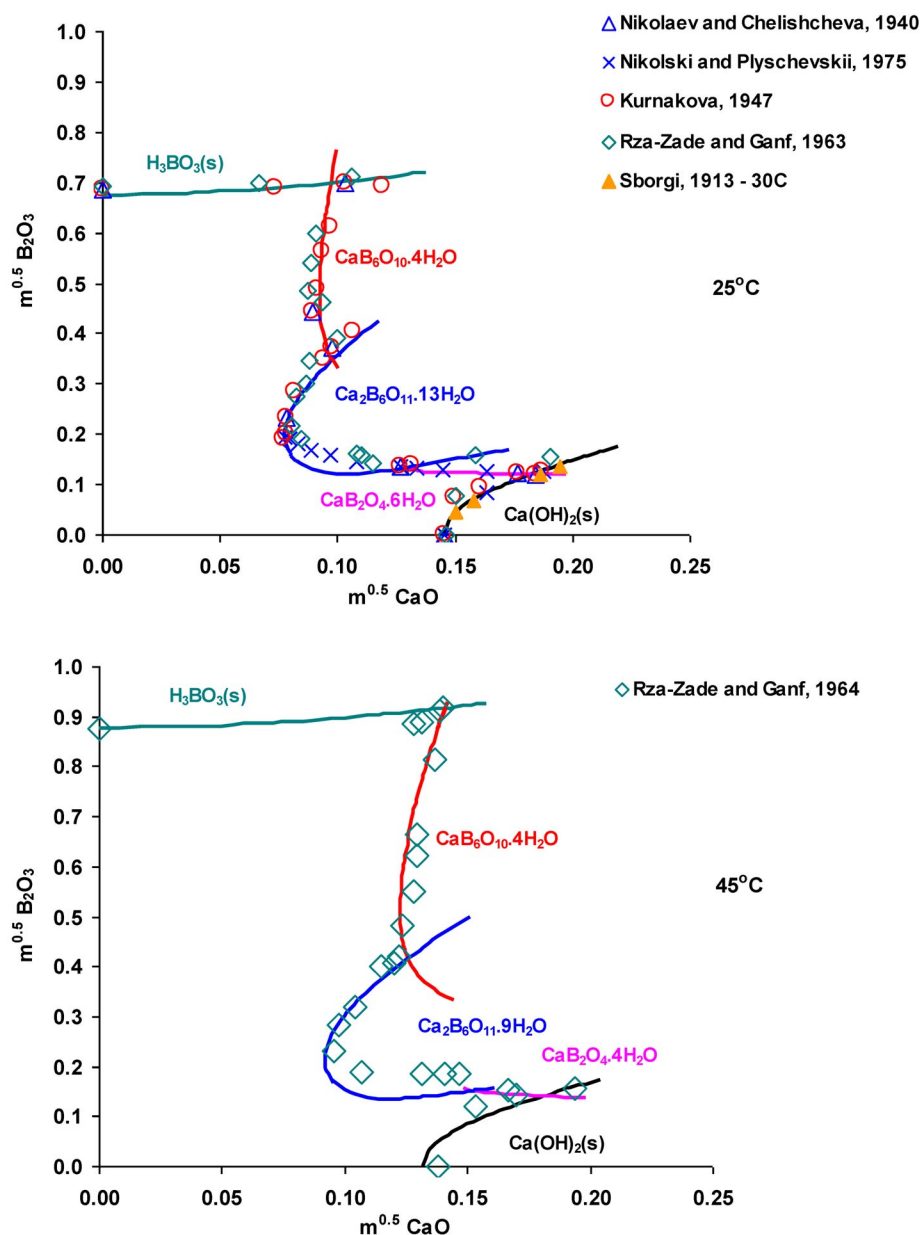
Fig. 10 Solubilities in the CaO + B_2O_3 + H_2O system at 25 and 45 °C. The symbols are literature data, and the lines are calculated using the MSE model.

Mixtures of boric acid and sodium borate with a chloride salt or an acid

The systems in this group include the ternary mixtures of H_3BO_3 + MCl + H_2O where M = Na, Li, or H, and the ternary or higher-order systems defined as ($NaBO_2$ or NaB_5O_8) + NaCl + H_2O, H_3BO_3 + NaOH + NaCl + H_2O, and $Na_2B_4O_7$ + $NaBO_2$ + H_3BO_3 + NaCl + H_2O. Table 4 summarizes the literature solubility data that were analyzed for these systems.

As the concentrations of the chloride salt or acid reach elevated levels in a system (i.e., up to ~19 molal HCl or solid saturation for LiCl and NaCl), it can be expected that solubilities are strongly

affected by ion interactions between the chloride ion and the prevailing boron species, in addition to those between the cation and the Cl⁻ ion and boron species as described above. Indeed, the model has been found to reproduce the solubility behavior of these systems by introducing ion interaction parameters between the Cl⁻ ion and various boron species that are present in significant amounts based on speciation analysis. These boron species include $H_3BO_{3(aq)}$, $HBO_{2(aq)}$, and polyborate anions as well as the associated ion pair $NaB(OH)_{4(aq)}$. In addition, the solubility behavior in the $H_3BO_3 + HCl + H_2O$ system has been found to be accurately represented when ion interaction parameters are introduced for the pair $H_3BO_{3(aq)}/H_3O^+$. This interaction has been found to have little or no effect on the results for other boron systems as described in previous sections, including the boric acid + water system, for which any ionic concentrations are at a minimal level due to the weak Lewis acid character of H_3BO_3. The binary interaction parameters determined for the chloride-containing systems can be found in Table 7 together with those for other systems. It should be noted that the interaction parameters determined for the boric acid/borate systems as described above are also included in the calculation of the solubilities for the chloride-containing systems because they pertain to all borate systems. The solid phases that are in equilibrium with solutions in the chloride-containing systems include $H_3BO_3(s)$ (in the $H_3BO_3 + MCl + H_2O$ ternaries) and various hydrates of sodium borates. Additionally, a double salt, $NaBO_2 \cdot NaCl \cdot 2H_2O$, has been found to precipitate at intermediate NaCl concentrations in the $NaBO_2 + NaCl + H_2O$ system [62]. The standard thermochemical properties of this solid phase are included in Table 6.

Results for the chloride-containing systems are shown in Figs. 11–13. The calculated and experimental solubilities are compared in Fig. 11 for the systems $NaBO_2 + NaCl + H_2O$ and $NaB_5O_8 + NaCl + H_2O$ at 20 °C. The stoichiometric ratio B:Na has a significant effect on the solubilities and their variation with NaCl concentration. The precipitated solids are also largely dependent on the B:Na ratio in the aqueous system. The solids that preferentially precipitate have a B:Na ratio that is similar to that in the aqueous solution. Thus, in the $NaBO_2 + NaCl + H_2O$ system, $Na_2B_2O_4 \cdot 8H_2O$ precipitates below a NaCl concentration of ~3.7 m. As the NaCl concentration increases, a double salt hydrate,
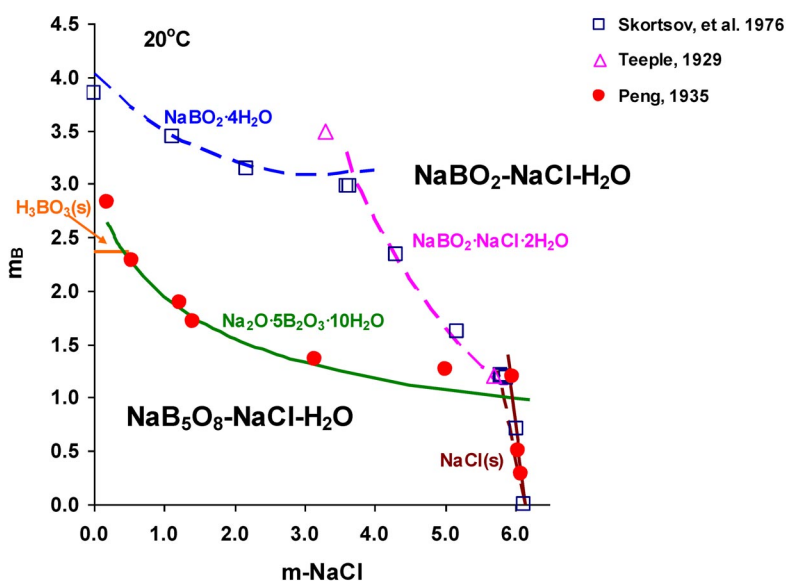
Fig. 11 Effect of NaCl concentration on the solubilities (expressed as total boron molality, m_B) in the $NaBO_2 + NaCl + H_2O$ (upper dashed curves) and $NaB_5O_8 + NaCl + H_2O$ (lower solid curves) systems at 20 °C. The symbols are literature data, and the lines are calculated using the MSE model.

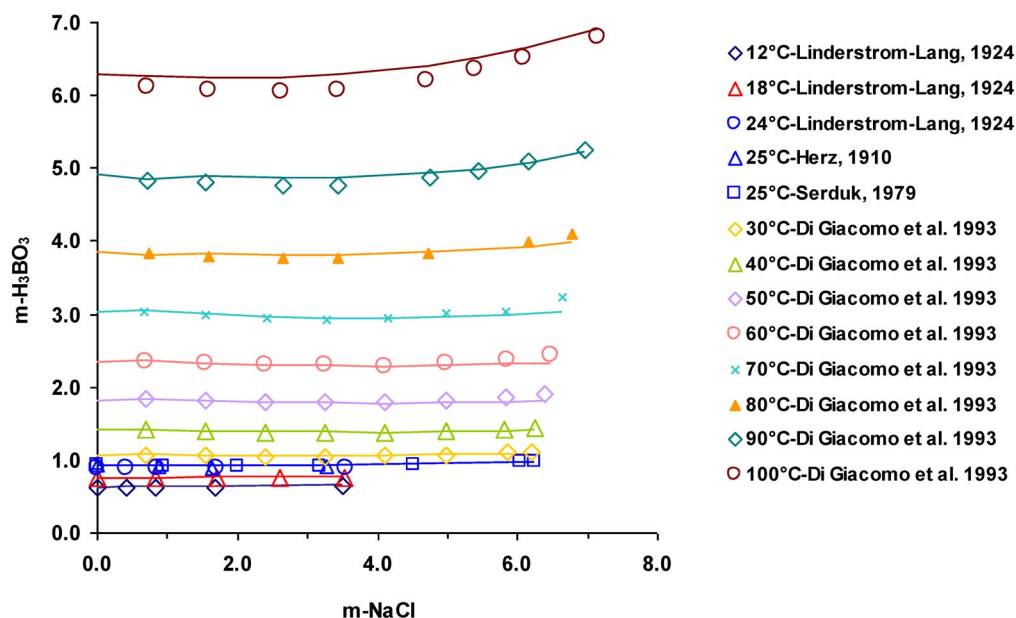**Fig. 12** Solubilities of $H_3BO_3(s)$ in aqueous NaCl solutions at various temperatures as a function of NaCl concentration. The symbols are literature data, and the lines are calculated using the MSE model.
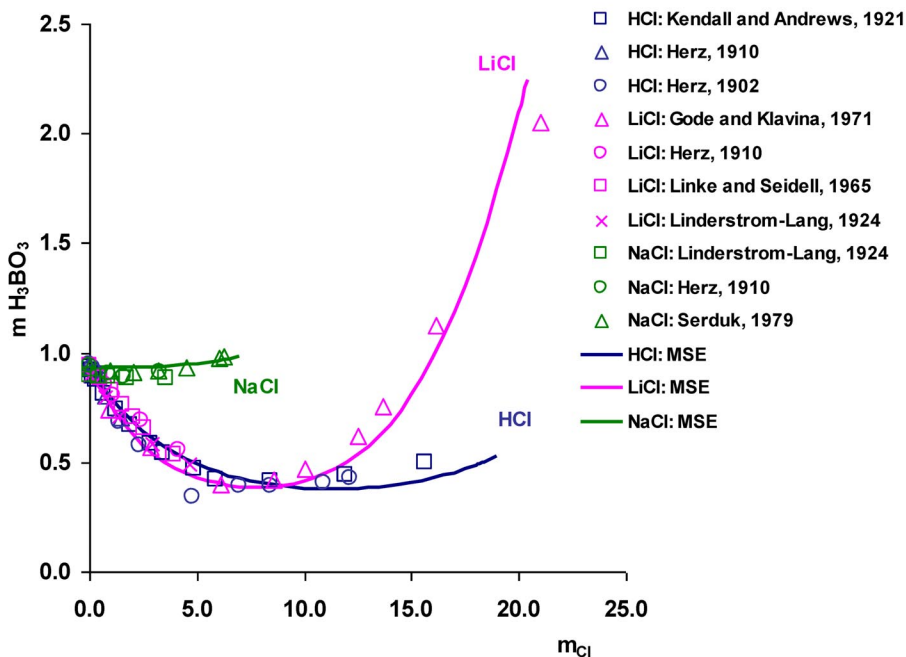
Fig. 13 Effect of chloride concentration on the solubility of $H_3BO_3(s)$ in aqueous NaCl, LiCl, and HCl solutions at 25 °C. The symbols are literature data, and the lines are calculated using the MSE model.

$NaBO_2 \cdot NaCl \cdot 2H_2O$ can precipitate before NaCl(s) becomes saturated at higher concentrations. For the $NaB_5O_8 + NaCl + H_2O$ system, due to a high B:Na ratio (5:1), $H_3BO_3(s)$ can precipitate at low NaCl

concentrations ($m_{NaCl} < 0.45$). A solid phase, $Na_2O \cdot 5B_2O_3 \cdot 10H_2O$, then precipitates over a wide range of NaCl concentration. The saturation curve of NaCl(s) is reached at a concentration that is close to the solubility of NaCl in pure water, and does not vary significantly with the total boron concentration. Figure 12 shows the effect of the NaCl concentration on the solubility of H_3BO_3(s) at various temperatures. It can be noted that temperature has the biggest effect on the solubility of H_3BO_3(s) while the effect of NaCl concentration is minimal in this system, especially at lower temperatures (i.e., below 80 °C). The effect of chloride ions on the solubility of H_3BO_3(s) can vary in different chloride solutions. This is illustrated in Fig. 13 where solubilities in three chloride solutions (i.e., LiCl, NaCl, and HCl) are compared. At low concentrations in LiCl and HCl solutions, the solubilities of H_3BO_3(s) decrease significantly with chloride concentration. After a minimum is reached, they rise with a further increase in chloride concentration. This increase is more pronounced in the LiCl solution compared to the HCl solution. In contrast to LiCl and HCl, the effect of NaCl on the H_3BO_3(s) solubility is slight as shown in Fig. 12. For NaCl, the solubility curve is nearly horizontal on the $m_{H_3BO_3}$ vs. m_{NaCl} diagram up to the NaCl saturation. These trends in the solubility behavior of H_3BO_3(s) reveal large differences in ionic interactions as chloride concentration changes in these systems. Overall, the effect of chlorides on the solubility of boric acid and various sodium borates is accurately represented by the MSE model.

CONCLUSIONS

Phase equilibria, speciation, and other thermodynamic properties of boric acid and aqueous binary and multicomponent lithium, sodium, magnesium, and calcium borate systems have been analyzed using the MSE model. One of the key advantages of this model is its ability to reproduce the properties of mixtures in which any component may continuously vary from being a solute to being a solvent. This capability of the MSE model has been demonstrated by accurately reproducing the solubilities in the $H_3BO_3/B_2O_3 + H_2O$ system over the complete composition range. The combination of an activity coefficient model with a comprehensive treatment of chemical equilibria in the MSE model makes it possible to represent simultaneously chemical speciation, phase equilibria, and other thermodynamic properties in an electrolyte system. This has been verified by calculating the pH, solubilities, and VLE for selected boron-containing systems and by predicting the effects of chemical speciation, temperature, and acid/base/salt concentrations on the formation of various solid phases.

ACKNOWLEDGEMENTS

REFERENCES

1. H. Corti, R. Crovetto, R. Fernandez-Prini. *J. Chem. Soc., Faraday Trans. 1* **76**, 2179 (1980).
2. D. A. Palmer, P. Benezeth, D. J. Wesolowski. *Power Plant Chem.* **2**, 261 (2000).
3. C. F. Baes, R. E. Mesmer. *The Hydrolysis of Cations*, John Wiley, New York (1976).
4. R. E. Mesmer, C. F. Baes, F. H. Sweeton. *Inorg. Chem.* **11**, 537 (1972).
5. Y. Zhou, C. Fang, Y. Fang, F. Zhu. *Spectrochim. Acta, Part A* **83**, 82 (2011).
6. Y. Jia, S. Gao, S. Xia, J. Li. *Spectrochim. Acta, Part A* **56**, 1291 (2000).
7. A. Anderko, P. M. Wang, M. Rafal. *Fluid Phase Equilib.* **194–197**, 123 (2002).
8. J. R. Loehe, M. D. Donohue. *AIChE J.* **43**, 180 (1997).
9. P. M. Wang, A. Anderko, R. D. Young. *Fluid Phase Equilib.* **203**, 141 (2002).
10. P. Wang, R. D. Springer, A. Anderko, R. D. Young. *Fluid Phase Equilib.* **222–223**, 11 (2004).
11. P. Wang, A. Anderko, R. D. Springer, R. D. Young. *J. Mol. Liq.* **125**, 37 (2006).
12. K. S. Pitzer. *Activity Coefficients in Electrolyte Solutions*, CRC Press, Boca Raton (1991).

13. P. Wang, A. Anderko, R. D. Young, R. D. Springer. In *35th Annual Hydrometallurgy Meeting*, D. G. Dixon, M. J. Dry (Eds.), pp. 259–273, Canadian Institute of Mining, Metallurgy and Petroleum, Montreal, Canada (2005).

14. M. S. Gruszkiewicz, D. A. Palmer, R. D. Springer, P. M. Wang, A. Anderko. *J. Solution Chem.* **36**, 723 (2007).

15. J. J. Kosinski, P. M. Wang, R. D. Springer, A. Anderko. *Fluid Phase Equilib.* **256**, 34 (2007).

16. H. Liu, V. G. Papangelakis. *Fluid Phase Equilib.* **234**, 122 (2005).

17. H. Liu, V. G. Papangelakis. *Ind. Eng. Chem. Res.* **45**, 39 (2006).

18. G. Azimi, V. G. Papangelakis, J. E. Dutrizac. *Fluid Phase Equilib.* **260**, 300 (2007).

19. G. Azimi, V. G. Papangelakis, J. E. Dutrizac. *Fluid Phase Equilib.* **266**, 172 (2008).

20. P. M. Wang, A. Anderko. *Fluid Phase Equilib.* **302**, 74 (2011).

21. D. S. Abrams, J. M. Prausnitz. *AIChE J.* **21**, 116 (1975).

22. H. C. Helgeson, D. H. Kirkham, G. C. Flowers. *Am. J. Sci.* **274**, 1089 (1974).

23. H. C. Helgeson, D. H. Kirkham, G. C. Flowers. *Am. J. Sci.* **276**, 97 (1976).

24. H. C. Helgeson, D. H. Kirkham, G. C. Flowers. *Am. J. Sci.* **281**, 1241 (1981).

25. E. L. Shock, H. C. Helgeson. *Geochim. Cosmochim. Acta* **52**, 2009 (1988).

26. D. A. Sverjensky, E. L. Shock, H. C. Helgeson. *Geochim. Cosmochim. Acta* **61**, 1359 (1997).

27. W. C. Blasdale, C. M. Slansky. *J. Am. Chem. Soc.* **61**, 917 (1939).

28. M. Chanson, F. J. Millero. *J. Solution Chem.* **35**, 689 (2006).

29. M. P. Dukelski. *Z. Anorg. Chem.* **50**, 38 (1906).

30. H. Menzel. *Z. Anorg. Allg. Chem.* **164**, 1 (1927).

31. A. Benrath. *Z. Anorg. Allg. Chem.* **249**, 245 (1942).

32. L. McCulloch. *J. Am. Chem. Soc.* **59**, 2650 (1937).

33. R. Nasini, J. Ageno. *Z. Phys. Chem.* **69**, 482 (1910).

34. N. P. Nies, R. W. Hulbert. *J. Chem. Eng. Data* **12**, 303 (1967).

35. R. F. Platford. *Can. J. Chem.* **47**, 2271 (1969).

36. F. C. Kracek, G. W. Morey, H. E. Merwin. *Am. J. Sci.* **35**, 143 (1938).

37. J. A. Kukuljan, J. L. Alvarez, R. Fernández-Prini. *J. Chem. Thermodyn.* **31**, 1511 (1999).

38. M. von Stackelberg, F. Quatram, J. Dressel. *Z. Elektrochem. Ang. Phys. Chem.* **43**, 14 (1937).

39. D. D. Macdonald, S. Hettiarachchi, H. Song, K. Makela, R. Emerson, M. Benhaim. *J. Solution Chem.* **21**, 849 (1992).

40. D. D. Macdonald, P. R. Wentrcek, A. C. Scott. *J. Electrochem. Soc.* **127**, 1745 (1980).

41. I. M. Abdulagatov, N. D. Azizov. *J. Solution Chem.* **33**, 1305 (2004).

42. O. S. Alekhin, S. V. Tsai, V. N. Gilyarov, L. V. Puchkov, V. I. Zarembo. *Z. Prikl. Khim.* **66**, 441 (1993).

43. J. G. Ganopolsky, H. L. Bianchi, H. R. Corti. *J. Solution Chem.* **25**, 377 (1996).

44. L. Hnedkovsky, V. Majer, R. H. Wood. *J. Chem. Thermodyn.* **27**, 801 (1995).

45. G. K. Ward, F. J. Millero. *J. Solution Chem.* **3**, 431 (1974).

46. D. D. Wagman, W. H. Evans, V. B. Parker, R. H. Schumm, I. Halow, S. Bailey, K. L. Churney, R. L. Nuttal. *J. Phys. Chem. Ref. Data* **11**, 2 (1982).

47. J. B. Farmer. In *Advances in Inorganic Chemistry and Radiochemistry*, H. J. Emeleus, A. G. Sharpe (Eds.), pp. 187–237, Academic Press, New York (1982).

48. L. Haar, J. S. Gallagher, G. S. Kell. *NBS/NRC Steam Tables: Thermodynamic and Transport Properties and Computer Programs for Vapor and Liquid States in SI Units*, Hemisphere Publishing, Washington, DC (1984).

49. G. K. Ward, F. J. Millero. *J. Solution Chem.* **3**, 417 (1974).

50. A. J. Ellis, I. M. McFadden. *Geochim. Cosmochim. Acta* **36**, 413 (1972).

51. M. W. J. E. Chase. *J. Phys. Chem. Ref. Data Monograph* **9**, 1 (1998).

52. J.-Z. Yang, P.-S. Song, D.-B. Wang. *J. Chem. Thermodyn.* **29**, 1343 (1997).

53. H. R. Corti, R. Crovetto, R. Fernandez-Prini. *J. Solution Chem.* **9**, 617 (1980).
54. G. S. Pokrovski, J. Schott, A. S. Sergeyev. *Chem. Geol.* **124**, 253 (1995).
55. L. M. Rowe, G. Atkinson. *J. Solution Chem.* **19**, 149 (1990).
56. J.-Z. Yang, B. Sun, P.-S. Song. *Thermochim. Acta* **352–353**, 69 (2000).
57. E. J. Reardon. *Chem. Geol.* **18**, 309 (1976).
58. I. Barin. *Thermochemical Data of Pure Substances*, VCH, Federal Republic of Germany (1989).
59. A. U. Sheleg, T. I. Dekola, N. P. Tekhanovich, A. M. Luginets. *Phys. Solid State* **39**, 545 (1997).
60. L. V. Gurvich, I. V. Veyts, C. B. Alcock. *Thermodynamic Properties of Individual Substances*, 4th ed., Hemisphere Publishing (1990).
61. W. T. Reburn, W. A. Gale. *J. Phys. Chem.* **59**, 19 (1955).
62. V. G. Skortsov, R. S. Tsekhanskii, A. M. Gavrilov. *Russ. J. Inorg. Chem.* **21**, 315 (1976).
63. A. P. Rollet, R. Bouaziz. *Comptes Rendus* **240**, 1227 (1955).
64. R. Bouaziz. *Ann. Chim. (France)* **6**, 345 (1961).
65. A.-Y. Zhang, Y. Yao, L.-J. Li, P.-S. Song. *J. Chem. Thermodyn.* **37**, 101 (2005).
66. S. H. Sang, H. A. Yin, M. L. Tang, N. F. Lei. *J. Chem. Eng. Data* **49**, 1586 (2004).
67. H. Menzel. *Z. Anorg. Allg. Chem.* **164**, 22 (1927).
68. H. Menzel. *Z. Anorg. Allg. Chem.* **166**, 63 (1927).
69. W. A. Byers, W. T. Lindsay, R. H. Kunig. *J. Solution Chem.* **29**, 541 (2000).
70. F. Linke, A. S. Seidell (Eds.). *Solubilities of Inorganic and Metal-organic Compounds*, American Chemical Society, Washington, DC (1965).
71. A. Rosenheim, F. Leyser. *Z. Anorg. Allg. Chem.* **119**, 1 (1921).
72. H. P. Rothbaum, H. J. Todd, I. K. Walker. *J. Chem. Eng. Data* **1**, 95 (1956).
73. O. Weres. *J. Solution Chem.* **24**, 409 (1995).
74. M. A. Urusova, V. M. Valyashko. *Russ. J. Inorg. Chem.* **35**, 719 (1990).
75. P. H. Kemp. Borax Consolidated Limited, London (1956).
76. A. Apelblat, E. Manzurola. *J. Chem. Thermodyn.* **35**, 221 (2003).
77. H. Menzel, H. Schulz. *Z. Anorg. Allg. Chem.* **251**, 167 (1943).
78. J. E. Teeple. *The Industrial Development of Searles Lake Brines - with Equilibrium Data*, The Chemical Catalog Company (1929).
79. V. P. Mashovets, L. V. Puchkov, S. N. Sidorova, M. K. Fedorov. *J. Appl. Chem. USSR* **47**, 548 (1974).
80. A. G. Kurnakova. *Izvest. Sektora Fiz. Khim. Anal., Inst. Obshchei i Neorg. Khim., Akad. Nauk SSSR* **15**, 125 (1947).
81. P. F. Rza-Zade, K. L. Ganf. *Azerb. Khim. Zh.* **3**, 120 (1963).
82. P. F. Rza-Zade, K. L. Ganf. *Azerb. Khim. Zh.* **6**, 92 (1964).
83. A. V. Nikolaev, A. G. Chelishcheva. *Dokl. Akademii Nauk SSSR* **28**, 127 (1940).
84. R. Mandelbaum. *Z. Anorg. Chem.* **62**, 370 (1909).
85. B. A. Nikolskii, Y. S. Plyschevskii. *Z. Neorg. Khim.* **20**, 2231 (1975).
86. U. Sborgi. *Atti Accad. Lincei* **22**, 716 (1913).
87. P. F. Rza-Zade, G. Bagirov, G. S. Sedelnikov. *Azerb. Khim. Zh.* **2**, 117 (1964).
88. P. F. Rza-Zade, R. A. Abduragimova, G. S. Sedelnikov, A. Afuzova. *Akad. Nauk Azerb. SSR, Inst. Neorg. Fiz. Khim.* **71**, 69 (1966).
89. J. D'Ans, K. H. Behrendt. *Kali Steinsalz* **2**, 121 (1957).
90. K. Linderstrom-Lang. *Compt. Rend. Trav. Lab. Carlsberg* **15**, 20 (1924).
91. G. Di Giacomo, P. Brandani, V. Brandani, G. Del Re. *Desalination* **91**, 21 (1993).
92. W. Herz. *Z. Anorg. Chem.* **66**, 358 (1910).
93. V. V. Serduk. *Russ. J. Phys. Chem. (in Russian)* **53**, 419 (1979).
94. H. Gode, L. Klavina. *Russ. J. Inorg. Chem.* **16**, 1794 (1971).
95. J. Kendall, J. C. Andrews. *J. Am. Chem. Soc.* **43**, 1545 (1921).
96. W. Herz. *Z. Anorg. Chem.* **33**, 355 (1902).

 97. C.-M. Peng. *Bull. Soc. Chim. France* **2**, 985 (1935).
 98. P. Y. Kuka, G. K. Gode. *Izv. AN Latv. SSR, Ser. Khim.* **2**, 245 (1969).
 99. H. L. Johnston, E. C. Kerr. *J. Am. Chem. Soc.* **72**, 4733 (1950).
100. D. R. Stull, D. L. Hildenbrandt, F. L. Oetting, G. C. Sinke. *J. Chem. Eng. Data* **15**, 52 (1970).
101. T. W. Bauer, H. L. Johnston, E. C. Kerr. *J. Am. Chem. Soc.* **72**, 5174 (1950).
102. R. A. Robie, B. S. Hemingway. In *U.S. Geological Survey Bulletin 2131* (1995).
103. V. P. Glushko, L. V. Gurvich, G. A. Bergman, I. V. Veyts, V. A. Medvedev, G. A. Kchachkurusov, B. S. Yungman. *Thermodynamic Properties of Individual Substances*, Nauka, Moscow (1982).
104. J. E. Hurst, B. K. Harrison. *Chem. Eng. Commun.* **112**, 21 (1992).